Cardiosphere-derived exosomal microRNAs for myocardial repair in pediatric dilated cardiomyopathy

Kenta Hirai[1], Daiki Ousaka[2], Yosuke Fukushima[1], Maiko Kondo[1], Takahiro Eitoku[1], Yusuke Shigemitsu[1], Mayuko Hara[1], Kenji Baba[1], Tatsuo Iwasaki[3], Shingo Kasahara[2], Shinichi Ohtsuki[1], and Hidemasa Oh[4]*

Departments of Pediatric Cardiology[1], Cardiovascular Surgery[2], and Anesthesiology and Resuscitology[3], Okayama University Graduate School of Medicine, Dentistry, and Pharmaceutical Sciences; Department of Regenerative Medicine[4], Center for Innovative Clinical Medicine, Okayama University Hospital, 2-5-1 Shikata-cho, Kita-ku, Okayama 700-8558, Japan.

Single sentence summary: Cardiosphere-derived exosomes improve cardiac function in dilated cardiomyopathy and provide safety lead-in results for further clinical translation.

*****Corresponding author. E-mail: hidemasa@okayama-u.ac.jp

Overline: DILATED CARDIOMYOPATHY

Abstract

Although cardiosphere-derived cells (CDCs) improve cardiac function and outcomes in patients with single ventricle physiology, little is known about their safety and therapeutic benefit in children with dilated cardiomyopathy (DCM). We aimed to determine the safety and efficacy of CDCs in a porcine model of DCM and translate the preclinical results into this patient population. A swine model of DCM using intracoronary injection of microspheres created cardiac dysfunction. Forty pigs were randomized as preclinical validation of the delivery method and CDC doses, and CDC-secreted exosomes (CDCex)-mediated cardiac repair was analyzed. A phase 1 safety cohort enrolled 5 pediatric patients with DCM and reduced ejection fraction to receive CDC infusion. The primary endpoint was to assess safety, and the secondary outcome measure was change in cardiac function. Improved cardiac function and reduced myocardial fibrosis were noted in animals treated with CDCs compared with placebo. These functional benefits were mediated via CDCex that were highly enriched with proangiogenic and cardioprotective microRNAs (miRNAs), whereas isolated CDCex did not recapitulate these reparative effects. One-year follow-up of safety lead-in stage was completed with favorable profile and preliminary efficacy outcomes. Increased CDCex-derived miR-146a-5p expression was associated with the reduction in myocardial fibrosis via suppression of proinflammatory cytokines and transcripts. Collectively, intracoronary CDC administration is safe and improves cardiac function through CDCex in a porcine model of DCM. The safety lead-in results in patients provide a translational framework for further studies of randomized trials and CDCex-derived miRNAs as potential paracrine mediators underlying this therapeutic strategy.

INTRODUCTION

Dilated cardiomyopathy (DCM) in children is the most common form of pediatric cardiomyopathy and may manifest as diverse disorders with both acquired and genetic causes. Although the annual incidence of primary DCM in childhood is low, 5-year event-free survival from death or cardiac transplantation was estimated to be 50-60% (*1*). Because preclinical and clinical studies of heart failure therapies in patients with pediatric DCM have been limited by a lack of both suitable experimental models and sufficient statistical power to validate the endpoints due to the small sample sizes, few pharmacological treatments and nonpharmacological interventions have been developed to reduce mortality in children with advanced heart failure.

The potential use of stem cells to attenuate the progressive reduction in ventricular function with congenital heart disease (CHD) has been a topic of considerable interest (*2*). Over recent years, the mobilization and direct delivery of various types of stem cells has expanded the possibilities for myocardial repair to treat children with CHD including DCM; however, few studies have been conducted using prospective, controlled trials (*3*, *4*). Among the various types of stem cells applied in the pediatric population, intracoronary delivery of cardiosphere-derived cells (CDCs) has been shown to provide functional benefits over staged surgical palliations in children with single ventricle lesions (*5*-*7*). CDCs are intracardiac in origin and exhibit a heterogeneous population to form multicellular clusters composed of clonally-derived cells. Our initial results from the prospective phase 1 controlled study TICAP (Transcoronary Infusion of Cardiac Progenitor Cells in Single Ventricle Physiology) and randomized phase 2 controlled trial PERSEUS (Cardiac Progenitor Cell Infusion to Treat Univentricular Heart Disease)

substantiated the safety profile as well as the therapeutic efficacy of CDC infusion in patients with structural heart diseases, and the subsequent long-term cohort study demonstrated a favorable impact on improvements in cardiac function and clinical outcomes (*8*). A recent randomized trial suggested a possible beneficial effect of intracoronary allogeneic CDCs in adolescents with neuromuscular disorders (*9*). Given the differential responses associated with CDC delivery observed in children compared with those in adults, outcomes might be dependent on the disease and age-related regenerative potentials of CDCs, mostly mediated through their secreted extracellular vesicles (*10*, *11*). Whether patients with pediatric DCM benefit from CDC treatment remains elusive.

In the current study, we established a porcine model with a dilated left ventricle (LV) and global systolic dysfunction by coronary microembolization to recapitulate the structural and functional phenotypes of DCM. This preclinical model was instrumental in the evaluation of procedural safety and therapeutic efficacy of nonocclusive transcoronary infusion of CDCs in pigs as part of a randomized dose-escalation study. Our results demonstrated that blockade of exosome secretion from CDCs decreased the benefits from therapy with CDCs that lead to improved cardiac function, such as cardiomyocyte proliferation, enhanced angiogenesis, and reduced myocardial fibrosis. Based on these preclinical investigations, a prospective phase 1a study of intracoronary CDC infusion was conducted and evaluated in children with DCM and reduced ejection fraction (EF).

RESULTS

Generation of a swine model of DCM

The animal model of DCM was induced by microembolization through three-vessel intracoronary delivery of embolic microspheres (Fig. 1A). As an initial pilot study in 10 pigs, we first probed the stability of global LV dysfunction and interindividual variability using a dose titration test, which ranged from 0.5×10^4 to 1.5×10^4 microspheres. A total of 1.0×10^4 particles was determined for injection per animal based on the hemodynamic and functional responses to microsphere infusion. Mortality occurred in 5 out of 48 animals on the day of microsphere injection and 3 pigs were excluded because the ejection function did not decrease to less than 50%. Forty animals survived (83.3%) with dilated LV and reduced systolic function and were randomized for safety and efficacy evaluation studies (Fig. 1B). Two weeks after coronary embolization, LVEF was significantly depressed compared with baseline by echocardiogram (37.6 ± 3.1% vs 61.8 ± 3.5%, $P<0.001$; Fig. 1C). Both LV end-diastolic and end-systolic dimensions were likewise increased 2 weeks after microembolization ($P<0.001$; Fig. 1, D to F). Greater myocardial fibrosis was documented by Picrosirius red staining in perivascular and interstitial regions of the heart after microembolization compared with sham controls (17.5 ± 4.0% vs 0.9 ± 0.6%, $P<0.001$; Fig. 1G).

Safety and CDC dosing studies in DCM model

To examine the procedural safety and therapeutic effects of intracoronary CDC infusion in a DCM model, cardiac tissues were obtained from the swine right atrium and CDCs were isolated and expanded using an explant culture procedure as described previously (fig. S1A) (*12*). Immunofluorescent staining and fluorescence-activated cell sorting (FACS) analyses revealed that swine CDCs expressed typical mesenchymal stem cell markers as we reported previously in a human study (fig. S1, B and C) (*5*). Compared with heart tissue, swine CDCs had higher

expression of *GATA4*, insulin-like growth factor-1 (*IGF1*), and vascular endothelial growth factor A (*VEGFA*) but lacked the mature cardiac structural protein, cardiac troponin-I (*TNNI3*) (fig. S1D). To verify the procedural safety during intracoronary infusion of CDCs in a swine model of DCM, 0.9×10^7 CDCs were administered into three coronary arteries with or without balloon inflation. No animals died during CDC injection; however, CDC infusion by stop-flow procedure showed higher incidence of transient ischemia (P=0.008) and ventricular arrhythmia (P=0.048) compared with that by the non-stop-flow approach (table S1). A small increase in cardiac troponin-T and troponin-I concentrations was observed in both procedures but was limited within the peri-procedural range (fig. S2).

To determine the therapeutic dose of CDCs in a DCM model, animals were randomly assigned to be treated by either intracoronary infusion of phosphate-buffered saline (PBS) as placebo or different doses of CDCs (0.9×10^7 cells calculated based on 3.0×10^5/kg and 1.8×10^7 cells as 6.0×10^5/kg) using a nonocclusive procedure (fig. S3). The minimal cell dose for infusion was defined based on our previous clinical phase 1/2 trials conducted in patients with single ventricle congenital heart disease and adjusted by body weight (*5*, *7*). The absolute changes in LVEF, assessed by echocardiography and cardiac magnetic resonance imaging (cMRI) at 1 month after protocol treatment, were significantly increased in both low- and high-dose CDC-treated groups compared with that in placebo-treated animals (P<0.001 vs placebo; fig. S3A). By contrast, late gadolinium enhancement (LGE) on cMRI, as a quantifying measure for myocardial scar, decreased markedly in both the low- and high-dose CDC-treated groups relative to the placebo control (+1.1 ± 0.5% in placebo vs -4.6 ± 2.0% in low-dose CDCs vs -2.6 ± 0.7% in high-dose CDCs, P<0.001; fig. S3B). The reduction in myocardial scar after CDC

infusion compared with controls was confirmed using Picrosirius red staining and showed similar results (fig. S3C). These CDC treatment-derived functional benefits were closely associated with enhanced capillary density and increased cardiomyocyte proliferation, as assessed by von Willebrand factor, Ki67, and phosphorylation of histone H3 immunostainings, respectively (fig. S3, D to F).

CDC exosome-mediated cardiac repair

Exosomes have been described as small extracellular vesicles that are produced by a variety of cell types including stem cells and may function as a vehicle to transfer microRNA (miRNA), mRNA, and proteins for intercellular communication (*13*). To test the hypothesis that exosomes secreted by CDCs (CDCex) could induce profound beneficial effects observed during the regenerative processes in a DCM model, CDCex were isolated and their molecular signatures were confirmed by CD9, CD63, and CD81 protein expression (Fig. 2, A to C). Raft-associated protein Flotillin-1 was not enriched in CDCex compared with CDC lysate, and polymeric cytochrome *c* was completely absent in CDCex as previously described (*14*). Pretreatment with GW4869, a selective inhibitor of neural sphingomyelinase, for 12 hours decreased exosome release from CDCs in a dose-dependent manner without affecting either the cell viability or replicative capacity (Fig. 2, D to F). miRNA transcriptional profiling of CDCs and CDCex identified several miRNAs that were markedly enriched in CDCex ,included miR-126-5p, miR-132, miR-146a-5p, miR-181b, miR-210, and miR-451; those have been reported to induce antifibrotic, antiapoptotic, and proangiogenic properties via activation of endogenous cardiac repair mechanisms (Fig. 2G) (*15*). As a result of GW4869 treatment, CDCex showed a reduced secretory profile of these miRNAs, whereas their intracellular expressions remained unchanged.

To determine whether the therapeutic benefits of CDCs were mediated by the secretion of exosomes, CDCs pretreated with or without GW4869 were transplanted into DCM pigs. Blockade of exosome release abrogated the functional recovery and histological improvements by CDCs in contrast to those primed with dimethyl sulfoxide (DMSO) controls, which imparted the anticipated therapeutic benefits of CDCs (Fig. 3, A to C). Likewise, CDCs pretreated with GW4869 did not enhance vascular density or cardiomyocyte proliferation 1 month after CDC infusion (Fig. 3, D to F). To verify whether intracoronary administration of CDCex may recapitulate the therapeutic effects of CDCs in a DCM model, exosomes were isolated from a total of 0.9×10^7 CDCs and co-injected with same dose of GW4869-treated CDCs for 12 hours to replicate the extravasation of paracrine effectors in local microenvironment. As shown in Fig. 3, intracoronary delivery of CDCex failed to improve cardiac function (cMRI: +3.2 ± 1.9% in DMSO controls vs -0.4 ± 1.9% in CDCex infusion, P=0.009; Fig. 3A), attenuate myocardial fibrosis (LGE: -6.2 ± 1.7% in DMSO controls vs -0.8 ± 1.6% in CDCex infusion, P<0.001; Fig. 3B), or promote angiogenesis and cardiomyocyte proliferation (Fig. 3, D to F).

Secretary mechanisms of exosomes in hypoxic CDCs

Although isolated CDCex did not contain small membranous particles released from apoptotic bodies and were carefully analyzed by canonical exosome markers, manufactured CDCs ex vivo might have different secretory constituents from those of transplanted CDCs in vivo after certain forms of physiological stress and inflammatory processes. Whether the biological function of GW4869 might be affected under these pathophysiological circumstances after CDC infusion in an animal model of DCM remains to be tested. Our data demonstrated that CDCs briefly exposed to tumor necrosis factor (TNF)-α or hypoxic conditions resulted in an increase

in hypoxia-inducible factor (*HIF*)-*1A* expression, and this was not changed by GW4869 treatment but was reduced by acriflavine (ACF) treatment, a HIF-1 inhibitor (fig. S4A) (*16*). While the blockade of exosomal secretion from CDCs by ACF was evident by hypoxia for 12 hours, GW4869 conferred stable inhibitory effects on CDCex biosynthesis regardless the oxygen conditions in culture (fig. S4B). Mechanisms of CDCex-derived autocrine effects by growth factors were also analyzed and revealed that inhibition of HIF-1 by ACF but not GW4869 reduced VEGF protein concentration under normoxia or in response to hypoxia (fig. S4C). The concentration of insulin-like growth factor-1 (IGF1) and basic fibroblast growth factor (bFGF), which are known to be regulated by non-vesicular secretion (*17*), was unchanged in CDC culture medium treated with GW4869 or ACF (fig. S4, D and E). In addition, the basic regulatory functions for secretory miRNAs appeared to be similar in the presence of both exosome inhibitors (fig. S5). Consistent with previous work, our results confirmed the sphingolipid ceramide-dependent regulatory action of GW4869 on CDCex (*17*-*19*) and recapitulated the pathophysiological relevance of its secretory machinery of proteins and miRNAs in vitro.

Patient enrollment and characteristics

Our results from preclinical studies provided a clinically relevant large animal model of DCM to evaluate procedural safety of intracoronary infusion of CDCs using a nonocclusive approach and to assess functional improvement, with histological evidence of myocardial repair in CDC-treated pigs. Motivated by these results, we proceeded to investigate clinical safety and therapeutic efficacy of CDC infusion in children with DCM and reduced EF. Fourteen consecutive patients were assessed for eligibility, and 9 patients were excluded due to

pacemaker implantation, coexistence of type-B Wolff–Parkinson–White syndrome requiring catheter ablation, recovered cardiac function by intensive medication or cardiac resynchronization therapy, or advanced respiratory failure (Fig. 4 and table S2). Ultimately, 5 DCM patients with or without LV noncompaction (LVNC) participated in the TICAP-DCM phase 1a trial as a treatment group (aged 11.4 ± 6.7 years; table S3). Their baseline characteristics and medications were generally similar, except for children with LVNC who showed a trend for earlier onset of heart failure compared with those without LVNC (Table 1). One patient without LVNC had markedly reduced LVEF (12.2%) during enrollment, indicating eligibility for registration on the heart transplant listing, but this patient refused to wait for transplant due to religious reasons (Table 1).

Safety evaluation

All participants had evident reduced LVEF (<40%) assessed by echocardiogram and cMRI, as required for enrollment. Endomyocardial biopsy specimens were obtained from individual patient, minced into explants, cultured, and passaged 3 to 4 times to achieve the prespecified CDC dose (3.0×10^5/kg) within 31.8 ± 4.7 days for injection after quality control validation (fig. S6). Although creatine kinases remained below the safety threshold, 4 out of 5 serum concentrations of cardiac troponin-T and -I were minimally elevated 1 day after CDC infusion but diminished over the 6 months of follow-up (fig. S7). No incidence of thoracic ectopic tissue formation was observed by cardiac imaging and biomarker analyses. There was one case of transient ischemia associated with CDC infusion (Table 2). This patient had serious adverse events including advanced heart failure and lung infection within 24 hours after CDC injection and required temporary use of circulatory support for recovery. No patients died or had acute

coronary syndrome or sustained ventricular arrhythmia during 12 months of follow-up (Table 2).

Cardiac function and heart failure status

Inotropic therapy used in 2 patients during study enrollment could be discontinued after CDC infusion (Table 1). Although this TICAP-DCM phase 1a trial was not considered to detect therapeutic efficacy on the basis of statistical power estimation, cardiac function and heart failure status were evaluated from baseline to 6- and 12-months of follow-up after CDC infusion as preliminary results of secondary outcomes. Compared with baseline, there was a nonsignificant trend for improvements in LVEF assessed by cMRI at 6- and 12-months post CDC treatment (EF: 26.4 ± 7.8% at baseline vs 31.5 ± 10.2% at 6 months vs 31.8 ± 9.4% at 12 months; *P*=0.067, Fig. 5A). Both end-diastolic and end-systolic volumes did not differ from baseline over 12 months of follow-up (Fig. 5B, *P*=1.0; Fig. 5C, *P*=0.689, respectively). Quantitative analysis of LGE and native T1 mapping also supported that functional recovery might be mediated through a reduction in the extent of myocardial fibrosis (LGE: 3.0 ± 2.0% at baseline vs 2.4 ± 1.6% at 12 months; *P*=0.248, Fig. 5, D and E) and extracellular volume fraction in patients treated with CDCs (native T1: 1041.6± 60.4 ms at baseline vs 984.8 ± 39.3 ms at 12 months, *P*=0.025; Fig. 5, F and G). Echocardiographic measurements revealed that CDC infusion increased the LVEF at 12 months (EF: 28.5 ± 10.7% at baseline vs 33.0 ± 11.1% at 12 months, *P*=0.038; Fig. 5H), whereas both end-diastolic and end-systolic volumes remained unchanged (Fig. 5I, *P*=0.980; Fig. 5J, *P*=0.528, respectively). B-type natriuretic peptide (BNP) amount did not differ (BNP: 205.2 ± 350.2 pg/mL at baseline vs 186.2 ± 319.7 pg/mL at 12 months, *P*=0.255), accompanied with a nonsignificant trend of improvement in Ross and New

York University pediatric heart failure index (NYUPHFI) classifications from baseline during 12 months of observation (Ross score: 2.4 ± 1.1 at baseline vs 1.8 ± 1.3 at 12 months, *P*=0.135; NYUPHFI: 11.4 ± 6.9 at baseline vs 9.0 ± 6.3 at 12 months, *P*=0.306; Fig. 5, K to M).

CDCex-derived miRNAs and reduction of myocardial fibrosis in patients with DCM

To further assess how transplanted CDCs confer therapeutic benefits in enrolled participants, we performed miRNA analysis on the small RNA fraction of CDCs and CDCex isolated from individuals and compared with that of human cardiac fibroblasts (HCFs). Patient-derived CDCex exhibited high expressions of CD9, CD63, and CD81 as measured by flow cytometry (Fig. 6, A and B). Flotillin-1 was ubiquitously present in both CDC fractions (Fig. 6C) but polymeric cytochrome *c* was barely detected in CDCex. CDCex were enriched in several miRNAs that have been previously shown to exert cardioprotective effects (*15*). Among the transcriptional targets, 5 miRNAs were specifically enriched in CDCex, including miR-126-5p, miR-132-3p, miR-146a-5p, miR-181b, and miR-210-3p, whereas miR-451a was enriched in both CDCex and HCFex (Fig. 6D). We investigated whether the transcriptional expression of the individual CDCex-derived miRNAs correlated with cardiac functional improvement after CDC treatment. The expressions of exosomal miR-146a-5p, but not miR-451a, were positively correlated with the reduction in both myocardial fibrosis (*r*=0.886, *P*=0.045) and extracellular volume fraction (*r*=0.896, *P*=0.040) at 12 months of follow up (Fig. 6E and fig. S8A).

miR-146a-5p inhibits inflammatory responses in human cardiomyocytes

To gain further insight into the physiological role of miR-146a-5p in myocardial inflammation and fibrosis, human AC16 cardiac cells were stimulated with TNF-α, a potent proinflammatory mediator which has been shown to contribute to remodeling and heart failure in human dilated

cardiomyopathy (*20*). Undifferentiated AC16 cells exposed to TNF-α for 12 and 24 hours resulted in an increase in miR-146a-5p expression (fig. S8B). To better understand the functional effects of miR-146a-5p, human AC16 cells were transfected with either overexpressed miR-146a-5p (mimic), antagonized miR-146a-5p (antagomir), or corresponding transfection controls (fig. S8, C and D). Transduction of mimic miR-146a-5p but not antagomir miR-146a-5p reduced TNF-α-induced cardiac apoptosis relative to scramble control (16.3 ± 1.3% vs 30.7 ± 6.1%: P=0.003; Fig. 6F and fig. S8E). TNF-α activated proinflammatory cytokines such as *interleukin (IL)-6* that was inhibited by miR-146a-5p overexpression but enhanced by antagomir to miR-146a-5p compared with controls (Fig. 6G and fig. S8F). On the other hand, miR-146a-5p reduced the expression of TNF receptor-associated factor 6 (*TRAF6*), *SMAD4*--a central mediator of transforming growth factor (TGF)-β signaling, and proto-oncogene *FOS* in the presence or absence of TNF-α (Fig. 6G), whereas blocking the miR-146a-5p by antagomir blunted most of those biological effects (fig. S8F). However, miR-146a-5p-mediated post-transcriptional regulation of *FOS* expression after TNF-α stimulation was comparable between miR-146a-5p antagomir and control, probably through the autocrine transcriptional repression.

DISCUSSION

Pediatric DCM is a rare disease but has become a leading cause of advanced heart failure, constituting the largest subpopulation of patients undergoing heart transplantation (*21*). DCMs in adults and children have similar structural and functional manifestations but are characterized by distinct etiologies and varied outcomes (*22*). There have been several clinical trials focused

on adult DCM, whereas extrapolating the evidence for therapeutic efficacy from adults to children often failed to confirm the benefits, and some delivery modalities may be neither feasible nor safe in children (*23*). Idiopathic DCM is estimated to occur in 50-70% of children with DCM; however, preclinical studies constructed to advance cell therapies to treat patients with pediatric DCM are still at an early stage of development due to the difficulty of disease modeling in large animals and limited by a varied range of disease classifications in children (*24*). The strengths of our preclinical study compared with previous assessments of therapeutic efficacy in stem cells could be the modeling of secondary DCM in large animals, dose titration to determine optimal cell dosage, and defining the possible mechanisms contributing to cardiac repair in DCM.

Increasing investigation of the pediatric DCM population by genetic analysis may suggest intervention strategies and predict disease severity. Doxorubicin- or tachycardia-induced cardiomyopathies have been reported to reconstitute the pathogenesis of secondary DCM in large animal studies (*25, 26*). These two experimental models have the advantage of producing a physiologically and morphologically relevant DCM model that closely resembles humans, but sudden cardiac death was frequently observed during anthracycline overload (n=10, qualified survival rate: 30%), and tachycardia-induced systolic dysfunction (n=5, qualified survival rate: 100%) was reversible by terminating the chronic pacing in our pig experiments (reversibility: 80%). Although DCM secondary to global myocardial ischemia is common in adults rather than in children as a form of acquired atherosclerosis, the causes of pediatric dilated cardiomyopathy leading from acquired myocardial ischemia are relatively rare. There are some common aspects of ischemic pathogenesis, such as Kawasaki disease with coronary aneurysm or stenosis and

cardiac allograft vasculopathy from heart transplantation (*1*). The empirical results of our preclinical study by coronary vessel microembolization produced a highly reproducible microinfarction model with global myocardial remodeling. However, the major limitation of our study might be the differential nature of pathogenesis between ischemic and nonischemic DCM during the preclinical investigation towards clinical translation.

In contrast to ischemic DCM, patients with nonischemic DCM exhibit a greater amount of dysfunctional but viable myocardium with a lesser extent of myocardial fibrosis, which may contribute to adverse remodeling. This differential disease pathogenesis during heart failure progression may reflect distinct disease mechanisms between adult and pediatric DCMs and also suggest that cell therapy may be appropriate for children with DCM (*22*). Recent progress in clinical studies has raised pivotal questions with respect to the optimized cell dose and delivery modality for pediatric DCM (*27*). Whether cell infusion with interrupted coronary flow is necessary for therapeutic efficacy remains uncertain but has been shown to increase the risks of adverse coronary events. The study design of our preclinical investigation rigorously evaluated the procedural safety and therapeutic efficacy of a nonocclusive intracoronary infusion approach at prespecified endpoints in a clinically relevant large animal model of DCM. Our results are consistent with the previous study performed in a swine model of single vessel myocardial infarction (*28*). In addition, a dose-escalation study is essential for clinical translation but has been poorly defined in DCM models. Our data provide a strong rationale for the clinical dosage to deliver in patients with DCM and that is consistent with the cell dose applied in children with single ventricle physiology in the TICAP and PERSEUS phase 1/2 trials as we reported previously (*5*, *7*).

Cardiac functional improvements in our preclinical study were associated with enhanced angiogenesis, increased endogenous cardiomyocyte proliferation, and reduced myocardial fibrosis; however, these observations cannot be appreciated solely by the direct engraftment and differentiation of transplanted CDCs (*29*). From this perspective, the results of our preclinical study suggested that CDC-derived paracrine factors such as exosomes might exert therapeutic benefits during the processes of cardiac repair (*15*). Although determining the specific exosome content that might be involved in extracellular communication by high throughput analysis remains particular challenging, blunting exosome secretion from CDCs abrogated the beneficial effects in the transplanted DCM hearts, supporting our hypothesis that a subset of miRNA, mRNA, and proteins secreted through CDCs might participate in the process of functional recovery. The blockade of exosome secretion with GW4869 is independent of the endosomal sorting complexes required for transport machinery but regulated by a sphingolipid ceramide-dependent pathway (*18*). A plausible mechanism of cardiac repair processes through vesicular secretion that does not depend on the Golgi apparatus or a subset of cytokines and signaling substances released through non-vesicular pathways cannot be excluded (*17*).

Consistent with previous reports, our results also confirmed that intracoronary delivery of CDCex alone was not sufficient to reproduce the beneficial paracrine effects of CDCs, perhaps because of a lack of efficient cardiac lodging due to the vesicle size (*30*). The quick intracellular uptake of exosomes, which might be dependent on the interplay between cell source and target cells to uptake the circulating vesicles, results in rapid CDCex clearance within the heart (*31*). In this regard, exosome secretion directly from the delivered CDCs at the site of cardiac localization is essential to avoid their rapid dissemination to other organs. The failure to yield

sufficient uptake of biologically active exosomes within the heart after intracoronary delivery of CDCex is one of the limitations in our preclinical study. Notwithstanding, optimal CDCex-based therapies would warrant further development of advanced technologies to incorporate the exosomes with a specific binding partner within the cardiac niche to activate endogenous myocardial repair processes.

Recent studies demonstrated that CDCex enriched in miR-146a-5p inhibited myocyte apoptosis and fibrosis, enhanced neovascular formation, and augmented cardiac function after infarction (*19*, *32*). Moreover, exposure to CDCex enabled fibroblasts to alter their intrinsic biological signals into distinct miRNA signatures included miR-146a-5p as therapeutic cells to restore cardiac function after injury (*33*). miR-146a-5p has been reported as a negative feedback mediator of nuclear factor-κB signaling through the transcriptional targeting of downstream effector components of its activation, including *TRAF6* and IL-1 receptor associated kinase 1 (*IRAK1*) (*34*). *SMAD3/4* cooperated with *FOS* to activate transcription in response to TGF-β-mediated inflammatory signaling at heterodimeric *activator protein-1* binding site to exert potent effects on extracellular matrix remodeling (*35*). Consistent with this interpretation, increased intrinsic expression of miR-146a-5p in CDCex may have cardioprotective effects on inflammatory responses as an efficient CDC-based postconditioning in patients with DCM. Although our results demonstrated that miR-451a expression was similar in both HCFex and CDCex, its biological function might differ by the pathogenesis of cardiomyopathy (*36*, *37*). Therefore, careful investigation of the physiological state of the parental cell of origin as well as the constituents of the exosomal contents would be required to define their intrinsic functions in the diseased heart. Nevertheless, our preliminary efficacy results highlighted the importance of

CDCex carrying cardioprotective miRNAs as potential prognostic biomarkers for cell therapy (*38*).

Of particular note, CDC- and CDCex-mediated myocardial repair in vitro and in vivo has been shown to be dependent on the donor's age, suggesting that donor CDCs and CDCex from children rather than adults might be beneficial as therapeutic applications (*11*, *39*). A comprehensive characterization of CDCex cargo to uncover the pharmacokinetics of CDCex may offer a fundamental advantage to enhance therapeutic efficacy in the injured heart for therapeutic success in the future (*40*).

This TICAP-DCM phase 1a study was conducted as an open-label, pilot, prospective trial at a single center. Due to the low annual incidence of pediatric DCM, the study was inevitably closed with a final enrollment of 5 participants out of a prespecified total of 7 without control patients for longitudinal comparison and limited to validation of the procedural feasibility and safety of intracoronary delivery of CDCs in children. The heterogenous population of patients with DCM with mixed cardiac phenotypes or diagnosed with insufficient genetic screening might also affect the safety profile and therapeutic responses after CDC infusion (*41*, *42*). Of the 5 children with DCM, minimal Troponin-T and -I elevations were observed within the peri-procedural range in 4 patients. One had serious adverse events, including congestive heart failure and lung infection, and required acute circulatory support for recovery after CDC infusion. This patient was at the highest risk of death and heart transplantation based on increased LV end-diastolic dimension, severity of LV dysfunction, and older age at diagnosis during study enrollment but refused wait listing for transplantation due to religious reasons (*43*,

44). Our experience has provided insights into an eligibility algorithm in children with intractable advanced heart failure without transplantation as a treatment option.

In our preclinical study, several mechanisms have been proposed to interpret the therapeutic benefit in children with DCM treated with CDCs, including increased neovascularization, myocyte proliferation, and reduction in myocardial fibrosis. Replacement fibrosis by cardiac scarring that developed in a discrete area of the myocardium as a result of myocyte cell death has been recognized as one of the pathological features of DCM. Although both LGE and T1-mapping measurements using cMRI have emerged as diagnostic methods to provide prognostic information of regional or diffuse myocardial disease for risk stratification, limited studies are available in children with heart disease (*45*). In our phase 1a clinical study, children with LVNC were excluded from quantitative T1-mapping analysis to measure the substantial fraction of myocardial extracellular volume, because the small and discrete regions of interest in thin ventricular wall segments with excessive trabeculations may lead to artificially high values. Conversely, pixel-wise mapping native T1 relaxation times were calculated to determine the degree of diffuse myocardial fibrosis (*46, 47*).

The preclinical study presented in this report was initiated to determine the clinically relevant optimal dosage of intracoronary delivered CDCs in a large animal model of DCM with widespread myocardial dysfunction. The procedural feasibility was confirmed using a nonocclusive coronary infusion approach with a satisfactory safety profile compared with conventional stop-flow delivery into 3 coronary arteries. CDC treatment in a DCM model was associated with improved myocardial function, increased neovascularization, cardiomyocyte proliferation, and reversed maladaptive changes manifested as cardiac fibrosis. These

therapeutic benefits could be completely abolished by blunting exosomal release of proangiogenic and cardioprotective miRNAs, including miR-146a-5p targeting of *TRAF6/SMAD4/FOS* for post-transcriptional repression, through the transplanted CDCs. Following rigorous preclinical investigations, the TICAP-DCM phase 1a trial was approved and conducted as a prospective clinical study with intracoronary infusion of CDCs in children with DCM. Our results during 1-year of follow-up indicate that CDCs are safe for the pediatric population and warrant continued study as an efficacy evaluation by the TICAP-DCM randomized-controlled phase 1b trial in children with DCM who have reduced ejection function but limited therapeutic options.

MATERIALS AND METHODS

Study design and outcome measures

The clinical study was registered as NCT03129568 (ClinicalTrials.gov). Individual subject-level data are provided in data file S1. The TICAP-DCM (Transcoronary Infusion of Cardiac Progenitor Cells in Pediatric Dilated Cardiomyopathy) phase 1, open-label trial was conducted at Okayama University Hospital between July 24th, 2017, and September 17th, 2018. The study design and protocol were approved by the Ethics Committee of Okayama University (01F1701003) and followed the Guidelines on Clinical Research Using Human Stem Cells issued by the Ministry of Health, Labour and Welfare, Japan. This trial was performed in accordance with the Declaration of Helsinki with written consent from all parents of eligible patients.

Children aged less than 18 years with a diagnosis of DCM based on clinical and echocardiographic findings were screened and the study enrollment required evidence of LV dilation with reduced EF defined as less than 40% (*1*). Although neuromuscular, mitochondrial, syndromic, and metabolic causes were considered to be further validated by genetic screening, sarcomeric mutation analysis was not performed in patients with cardiomyopathy with either isolated or LVNC phenotype. Exclusion criteria included cardiogenic shock, intractable arrhythmias, repeated infections, advanced renal or hepatic dysfunction, and manifested cancer diseases. Mixed hypertrophic or restrictive cardiomyopathy phenotypes were also excluded. Every eligible participant was subjected to endomyocardial biopsies to obtain sufficient specimens for pathological diagnosis and CDC culture. Patients classified as secondary DCM, such as inflammation, toxic exposure, metabolic disorders, and structural heart disease, were not enrolled in this trial.

The TICAP-DCM prospective, open-label, phase 1 trial comprised of a phase 1a study (n=5, prespecified as 7 but limited to 5 patients available for recruitment due to the disease severity and rarity) to evaluate procedural safety during intracoronary delivery of CDCs (3.0×10^5/kg) using nonocclusive approach, and a phase 1b study (n=24, in a 1:1 randomization) to assess the therapeutic benefits. The sample size was determined based on a power of 85% to detect a difference of 4.5% in the cardiac function, assuming that the common standard deviation is 3.5% between controls and CDC-treated groups using a 2-group *t* test at 2-sided. Study participants were assessed at baseline, 6, and 12 months of follow-up. The primary safety endpoint was adverse events occurring in the treatment arm including ventricular fibrillation, ventricular tachycardia, heart failure, myocardial infarction, advanced infection, and tumor

formation after CDC infusion (*5*). The secondary endpoint was to assess the functional improvement of the global cardiac function and heart failure status from baseline to 6 months of follow-up, as described previously (*7*). The study participants were closely monitored by an independent data monitoring committee at the Center for Innovative Clinical Medicine. Data management board at Translational Research Center for Medical Innovation (Kobe) has verified and vouched for the accuracy, completeness, and fidelity of the clinical data.

Animal model and randomization

The animal experimental protocols were approved by Okayama University Institutional Animal Care and Use Committee (OKU-2019058). All animals received humane animal care in compliance with the "Guide for the care and use of laboratory animals" published by Okayama University. Experiments were descriptive and exploratory without power consideration to determine the sample size. Fifty-eight female Yorkshire pigs of 25-35 kg in weight and at an age of 8-week-old were anesthetized by intramuscular injection of ketamine (10 mg/kg), xylazine (2 mg/kg), and atropine sulfate (0.5 mg), intubated, and placed on a ventilation system (ACOMA, PRO-45). Continuous sedation was maintained using a closed-circuit system with inhalation of 2% isoflurane. The DCM model characterized by global dilation and systolic dysfunction was generated by transcoronary injection of embolic agent that was made of tris-acrylic copolymer impregnated in porcine gelatin (Embosphere: 100–300 μm in diameter; Biosphere Medical) with modifications (*48*). A 6-French Hockey Stick or Judkins Right catheter (Medtronic, Minneapolis) was introduced and distal coronary selection was achieved using a high-flow type microcatheter (Akatsuki; Gadelius Medical). A total of 1.0×10^4 microspheres were dispersed in 15 mL of saline with 0.05% (vol/vol) Tween 80 and selectively

infused into three coronary arteries over 5 minutes for each injection (5 mL per coronary artery). Cardiac function was evaluated 2 weeks after microembolization, and qualified animals were randomly assigned to be treated by intracoronary infusion of PBS as placebo controls (n=5) or allogeneic CDCs (n=35) for cell dosing and function studies as indicated.

CDC delivery

Human and swine CDCs were isolated, manufactured, and validated as described in Supplementary Methods and table S4. Grown CDCs were resuspended in 0.1% heparin containing PBS in a total 15 mL volume and divided into 5 mL aliquots for each administration. In pig experiments, intracoronary injection of placebo or either 0.9×10^7 or 1.8×10^7 allogeneic CDCs was performed 2 weeks after coronary microembolization using a KUDOS balloon catheter (Fuji Systems) with either 3-minute balloon inflation (stop-flow procedure) or 5-minute deflation (nonocclusive procedure) cycles during three-vessel infusions. Myocardial ischemia was monitored by electrocardiogram and serum troponin-T/I measurement on the day and 24 hours after CDC infusion.

Histology

Paraffin-fixed ventricular rings were sectioned at 5 μm, deparaffinized, and stained with Picrosirius red (Polysciences, Warrington) and hematoxylin and eosin (H&E) to analyze the magnitude of cardiac fibrosis. Ten random images from each treatment group were captured and the percentage of myocardial fibrosis per image was quantified by using hybrid cell count system of BZ-X Analyzer. To evaluate microvascular density and myocyte proliferation, sections were stained with rabbit polyclonal antibodies against von Willebrand factor (ab6994), Ki67 (ab15580), or phospho-histone H3 (LS-C353149, LSBio) and a mouse monoclonal

antibody against myosin heavy chain (MA1-26180, Thermo Fisher Scientific) at 1:100 dilution. Alexa Fluor 488 goat anti-rabbit IgG, and Alexa Fluor 546 goat anti-mouse IgG (Thermo Fisher Scientific) were incubated as secondary antibodies (1:200 dilution), and nuclei were visualized with 4',6-diamidino-2-phenylindole (DAPI). The stained slides were evaluated in stacked images using a BZ-X710 Analyzer (KEYENCE).

Exosome preparation

CDCex isolation was performed as described previously with modifications (*30*). In brief, allogeneic swine or autologous human CDCs were washed and transferred to serum-free IMDM. After 48 hours, the conditioned medium was harvested, centrifuged for 20 minutes at 2,500 × g, and filtered through a 0.22 μm GV filter (Millex). The supernatant was transferred to an Ultra-15 centrifugal filter (10K; Amicon) after equilibration of the membrane with PBS by centrifugation at 4,000 × g for 10 minutes. CDCex were then isolated and concentrated by repeated centrifugation at 4,000 × g for 30 minutes and the exosomes pellet was resuspended in PBS solution for assays. CDCex obtained from 2.0×10^6 CDCs were diluted in 500 μl PBS and a total of 3 μl of CDCex-containing buffer was loaded onto a carbon-Formvar-coated copper grid, stained with uranyl acetate solution, and dried for scanning transmission electron microscopy (Hitachi H7650 TEM). The exosomes were characterized for size distribution and quantitated by NanoSight NS300 (Malvern Panalytical). CDCex inhibition was induced for 12 hours by either 20 μM GW4869 (Sigma-Aldrich), a selective inhibitor of neural sphingomyelinase, or 5 μM acriflavine (ACF; Sigma-Aldrich), a HIF-1 inhibitor. The cell viability was assessed using a trypan blue exclusion assay (Sigma Chemical Company).

Flow cytometric analysis

Swine CDCs were validated using the following primary and secondary antibodies: mouse monoclonal or rabbit polyclonal antibodies against CD90 (ab123511), CD105 (ab69772), CD31 (ab186720), and CD45 (ab10559); FITC-goat anti-mouse/rabbit antibodies (BD Pharmingen) and Alexa Fluor 546 or 488 goat anti-mouse/rabbit IgG (Thermo Fisher Scientific). Immunofluorescence and flow cytometric analysis (FACS) were performed in accordance with the methods used in human CDC validation (*5*). The human CDCex were validated by flow cytometry using an ExoCap Streptavidin Kit (MBL life science) according to the manufacturer's protocols. Magnetic microbeads coated with biotinylated-CD9, -CD63, or -CD81 antibodies were used to recognize the surface antigens. The fluorescent signals were detected by streptavidin-FITC conjugated antibody (Miltenyi Biotec Inc) using FlowJo. Microbeads incubated with an antibody in the absence of exosomes served as control. TNF-α (Cell Signaling Technology)-treated AC16 cells were double-stained with 5 μL annexin V and 5 μL propidium iodide using annexin V-FITC apoptosis detection kit (eBioscience) and myocardial apoptosis was evaluated by FACS.

Immunoblotting

The primary and secondary antibodies used for validation of CDC lysate or CDCex obtained from pigs and humans were as follows: rabbit polyclonal anti-CD9 (LS-C135937-100, LSBio); goat polyclonal anti-CD63 (ABIN1440014, antibodies-online Inc.); rabbit polyclonal anti-CD81 (AI14938, Abgent); goat polyclonal anti-Flotillin-1 (ab13493); rabbit polyclonal anti-cytochrome *c* (ab90529); mouse monoclonal anti-glyceraldehyde-3-phosphate dehydrogenase (GAPDH; ab8245); and goat anti-rabbit/horse anti-mouse (Cell Signaling Technology) /donkey anti-goat (Abcam) IgG HRP-linked antibodies.

Statistical analysis

Descriptive data are presented as absolute numbers and percentages or means and SDs. Significance of differences between two treatment groups was assessed using Student's *t*-test. Paired *t*-test was used to determine the significance between baseline and an endpoint within a group. For multiple comparisons of continuous measures between groups, the Kruskal-Wallis test was used if normality could not be established. When the variables were distributed normally, one-way analysis of variance (ANOVA) was performed and Tukey post hoc test was applied to determine the statistical significance between groups. Categorical variables presented by the number of observations between the groups were compared using Fisher exact test. Individual comparisons at baseline to 6 and 12 months of follow-up were analyzed by one-way ANOVA with repeated measures followed by Dunn–Bonferroni post hoc correction according to the data normality. The Friedman test was used to analyze the heart failure status in CDC-treated patients from baseline to 12 months of follow-up and Wilcoxon signed-rank test with Dunn–Bonferroni post hoc correction was applied to compare the changes from baseline. Linear regression analysis using Pearson's correlation coefficient was applied to evaluate the relationship between absolute changes in the extent of myocardial fibrosis from baseline to 12 months of follow up and the expressions of CDCex-derived miRNAs, and *r* values were presented as Pearson product-moment correlation coefficient. A *P* value less than 0.05 was considered to be significant. Analyses were conducted using SPSS software (version 26, IBM Corporation, Armonk, NY).

ACKNOWLEDGMENTS

We thank the members of the data management board at the Translational Research Center for Medical Innovation to vouch for the accuracy, completeness, and fidelity of the data; the safety monitoring and biostatistics board at Okayama University Hospital for providing critical review and statistical assistance to analyze the data; the entire project oversight committee, and all patients and their parents who gave consent to participate in this study.

FUNDING

This study was supported by grants from the Research Project for Practical Application of Regenerative Medicine (16bk0104052h0001, 17bk0104052h0002, 18bk0104052h0003) by the Japan Agency for Medical Research and Development (to H.O.) and Grant-in-Aid for Scientific Research (19H03738) by the Japan Society for the Promotion of Science (to H.O.).

AUTHOR CONTRIBUTIONS

H.O. was the chief clinical investigator for the study and contributed to the trial concept and design. K.H. and D.O. performed the cell culture and animal experiments. S.O. and H.O. contributed to the patient recruitment and oversaw the trial conduct. K.H. and H.O. collected the electronic data provided by the Translational Research Center for Medical Innovation and conducted data interpretation and statistical analyses. Y.F., M.K., T.E., Y.S., M.H., K.B., T.I., S.K., and S.O. performed catheter-based cell infusion and performed the protocol treatment on the enrolled patients. K.H. drafted the initial manuscript and H.O. wrote the manuscript.

COMPETING INTERESTS

H.O. has applied for a patent (JP4783909) and that was issued and licensed out to Japan Regenerative Medicine, which provided no funding for this study. The authors have declared that no conflict of interest exists.

DATA AND MATERIALS AVAILABILITY

All data associated with this study are present in the paper or the Supplementary Materials.

LIST OF SUPPLEMENTARY MATERIALS

Materials and Methods

Fig. S1. Isolation, expansion, and characterization of swine CDCs.

Fig. S2. Cardiac enzyme measurements during occlusive or nonocclusive delivery of CDCs in pigs.

Fig. S3. Dose-escalation study to assess CDC-mediated myocardial repair.

Fig. S4. Effects of GW4869 and HIF-1 inhibitor on exosome release and growth factors secretion to modulate adaptive responses to hypoxia.

Fig. S5. Hypoxic CDCs enhanced secretory miRNAs expressions those were repressed by GW4869 and ACF treatment.

Fig. S6. Isolation, expansion, and validation of human CDCs from endomyocardial biopsy specimens.

Fig. S7. Cardiac enzymes and tumor markers measurements for safety profile analysis (primary endpoint measures).

Fig. S8. The impact of miR-146a-5p on TNF-α-mediated autocrine and paracrine signaling against apoptosis in human cardiomyocytes.

Table S1. Adverse events during CDC delivery in swine model of DCM.

Table S2. Inclusion and exclusion criteria of the TICAP-DCM trial.

Table S3. Characteristics of study participants in the TICAP-DCM phase 1a trial.

Table S4. Taqman primers used for CDC and CDCex validation and function.

References (*49*)

Data file S1 (Microsoft Excel format). Individual subject-level data (separate file).

REFERENCES

1. S. E. Lipshultz, Y. M. Law, A. Asante-Korang, E. D. Austin, A. I. Dipchand, M. D. Everitt, D. T. Hsu, K. Y. Lin, J. F. Price, J. D. Wilkinson, S. D. Colan, Y. American Heart Association Council on Cardiovascular Disease in the, C. Council on Clinical, G. Council on, M. Precision, Cardiomyopathy in Children: Classification and Diagnosis: A Scientific Statement From the American Heart Association. *Circulation*, CIR0000000000000682 (2019).

2. H. Oh, Cell Therapy Trials in Congenital Heart Disease. *Circ Res* **120**, 1353-1366 (2017).

3. M. El-Shanshory, W. El-Shehaby, N. Hables, S. Hamad, M. Attia, A. El-Said, Study of peripheral stem cells mobilization as a treatment line of pediatric dilated cardiomyopathy. *Stem Cell Investig* **2**, 21 (2015).

4. D. I. Tsilimigras, E. K. Oikonomou, D. Moris, D. Schizas, K. P. Economopoulos, K. S. Mylonas, Stem Cell Therapy for Congenital Heart Disease: A Systematic Review. *Circulation* **136**, 2373-2385 (2017).

5. S. Ishigami, S. Ohtsuki, S. Tarui, D. Ousaka, T. Eitoku, M. Kondo, M. Okuyama, J. Kobayashi, K. Baba, S. Arai, T. Kawabata, K. Yoshizumi, A. Tateishi, Y. Kuroko, T. Iwasaki, S. Sato, S. Kasahara, S. Sano, H. Oh, Intracoronary autologous cardiac progenitor cell transfer in patients with hypoplastic left heart syndrome: the TICAP prospective phase 1 controlled trial. *Circ Res* **116**, 653-664 (2015).

6. S. Tarui, S. Ishigami, D. Ousaka, S. Kasahara, S. Ohtsuki, S. Sano, H. Oh, Transcoronary infusion of cardiac progenitor cells in hypoplastic left heart syndrome:

Three-year follow-up of the Transcoronary Infusion of Cardiac Progenitor Cells in Patients With Single-Ventricle Physiology (TICAP) trial. *J Thorac Cardiovasc Surg* **150**, 1198-1207, 1208 e1191-1192 (2015).

7. S. Ishigami, S. Ohtsuki, T. Eitoku, D. Ousaka, M. Kondo, Y. Kurita, K. Hirai, Y. Fukushima, K. Baba, T. Goto, N. Horio, J. Kobayashi, Y. Kuroko, Y. Kotani, S. Arai, T. Iwasaki, S. Sato, S. Kasahara, S. Sano, H. Oh, Intracoronary Cardiac Progenitor Cells in Single Ventricle Physiology: The PERSEUS (Cardiac Progenitor Cell Infusion to Treat Univentricular Heart Disease) Randomized Phase 2 Trial. *Circ Res* **120**, 1162-1173 (2017).
8. T. Sano, D. Ousaka, T. Goto, S. Ishigami, K. Hirai, S. Kasahara, S. Ohtsuki, S. Sano, H. Oh, Impact of Cardiac Progenitor Cells on Heart Failure and Survival in Single Ventricle Congenital Heart Disease. *Circ Res* **122**, 994-1005 (2018).
9. M. Taylor, J. Jefferies, B. Byrne, J. Lima, B. Ambale-Venkatesh, M. R. Ostovaneh, R. Makkar, B. Goldstein, R. R. Smith, J. Fudge, K. Malliaras, B. Fedor, J. Rudy, J. M. Pogoda, L. Marban, D. D. Ascheim, E. Marban, R. G. Victor, Cardiac and skeletal muscle effects in the randomized HOPE-Duchenne trial. *Neurology* **92**, e866-e878 (2019).
10. R. R. Makkar, R. R. Smith, K. Cheng, K. Malliaras, L. E. Thomson, D. Berman, L. S. Czer, L. Marban, A. Mendizabal, P. V. Johnston, S. D. Russell, K. H. Schuleri, A. C. Lardo, G. Gerstenblith, E. Marban, Intracoronary cardiosphere-derived cells for heart regeneration after myocardial infarction (CADUCEUS): a prospective, randomised phase 1 trial. *Lancet* **379**, 895-904 (2012).

11. L. Grigorian-Shamagian, W. Liu, S. Fereydooni, R. C. Middleton, J. Valle, J. H. Cho, E. Marban, Cardiac and systemic rejuvenation after cardiosphere-derived cell therapy in senescent rats. *Eur Heart J* **38**, 2957-2967 (2017).

12. R. R. Smith, L. Barile, H. C. Cho, M. K. Leppo, J. M. Hare, E. Messina, A. Giacomello, M. R. Abraham, E. Marban, Regenerative potential of cardiosphere-derived cells expanded from percutaneous endomyocardial biopsy specimens. *Circulation* **115**, 896-908 (2007).

13. R. Kishore, M. Khan, More Than Tiny Sacks: Stem Cell Exosomes as Cell-Free Modality for Cardiac Repair. *Circ Res* **118**, 330-343 (2016).

14. J. Kowal, G. Arras, M. Colombo, M. Jouve, J. P. Morath, B. Primdal-Bengtson, F. Dingli, D. Loew, M. Tkach, C. Théry, Proteomic comparison defines novel markers to characterize heterogeneous populations of extracellular vesicle subtypes. *Proc Natl Acad Sci U S A* **113**, E968-977 (2016).

15. V. N. S. Garikipati, F. Shoja-Taheri, M. E. Davis, R. Kishore, Extracellular Vesicles and the Application of System Biology and Computational Modeling in Cardiac Repair. *Circ Res* **123**, 188-204 (2018).

16. G. Cheloni, M. Tanturli, I. Tusa, N. Ho DeSouza, Y. Shan, A. Gozzini, F. Mazurier, E. Rovida, S. Li, P. Dello Sbarba, Targeting chronic myeloid leukemia stem cells with the hypoxia-inducible factor inhibitor acriflavine. *Blood* **130**, 655-665 (2017).

17. C. C. Glembotski, Expanding the Paracrine Hypothesis of Stem Cell-Mediated Repair in the Heart: When the Unconventional Becomes Conventional. *Circ Res* **120**, 772-774 (2017).

18. N. Kosaka, H. Iguchi, Y. Yoshioka, F. Takeshita, Y. Matsuki, T. Ochiya, Secretory mechanisms and intercellular transfer of microRNAs in living cells. *J Biol Chem* **285**, 17442-17452 (2010).

19. A. G. Ibrahim, K. Cheng, E. Marban, Exosomes as critical agents of cardiac regeneration triggered by cell therapy. *Stem Cell Reports* **2**, 606-619 (2014).

20. M. Satoh, M. Nakamura, H. Saitoh, H. Satoh, C. Maesawa, I. Segawa, A. Tashiro, K. Hiramori, Tumor necrosis factor-alpha-converting enzyme and tumor necrosis factor-alpha in human dilated cardiomyopathy. *Circulation* **99**, 3260-3265 (1999).

21. R. K. Singh, C. E. Canter, L. Shi, S. D. Colan, D. A. Dodd, M. D. Everitt, D. T. Hsu, J. L. Jefferies, P. F. Kantor, E. Pahl, J. W. Rossano, J. A. Towbin, J. D. Wilkinson, S. E. Lipshultz, I. Pediatric Cardiomyopathy Registry, Survival Without Cardiac Transplantation Among Children With Dilated Cardiomyopathy. *J Am Coll Cardiol* **70**, 2663-2673 (2017).

22. M. D. Patel, J. Mohan, C. Schneider, G. Bajpai, E. Purevjav, C. E. Canter, J. Towbin, A. Bredemeyer, K. J. Lavine, Pediatric and adult dilated cardiomyopathy represent distinct pathological entities. *JCI Insight* **2**, (2017).

23. B. Vrtovec, Cell Therapy for Nonischemic Cardiomyopathy: Current Status and Future Perspectives. *Circ Res* **122**, 28-30 (2018).

24. J. A. Towbin, A. M. Lowe, S. D. Colan, L. A. Sleeper, E. J. Orav, S. Clunie, J. Messere, G. F. Cox, P. R. Lurie, D. Hsu, C. Canter, J. D. Wilkinson, S. E. Lipshultz, Incidence, causes, and outcomes of dilated cardiomyopathy in children. *JAMA* **296**, 1867-1876 (2006).

25. S. Christiansen, A. Perez-Bouza, G. Schalte, R. D. Hilgers, R. Autschbach, Selective left ventricular adriamycin-induced cardiomyopathy in the pig. *J Heart Lung Transplant* **27**, 86-92 (2008).

26. P. Hala, M. Mlcek, P. Ostadal, D. Janak, M. Popkova, T. Boucek, S. Lacko, J. Kudlicka, P. Neuzil, O. Kittnar, Tachycardia-Induced Cardiomyopathy As a Chronic Heart Failure Model in Swine. *J Vis Exp*, (2018).

27. I. Michel-Behnke, I. Pavo, S. Recla, M. Khalil, C. Jux, D. Schranz, Regenerative therapies in young hearts with structural or congenital heart disease. *Transl Pediatr* **8**, 140-150 (2019).

28. E. Tseliou, H. Kanazawa, J. Dawkins, R. Gallet, M. Kreke, R. Smith, R. Middleton, J. Valle, L. Marban, S. Kar, R. Makkar, E. Marban, Widespread Myocardial Delivery of Heart-Derived Stem Cells by Nonocclusive Triple-Vessel Intracoronary Infusion in Porcine Ischemic Cardiomyopathy: Superior Attenuation of Adverse Remodeling Documented by Magnetic Resonance Imaging and Histology. *PLoS One* **11**, e0144523 (2016).

29. T. Eschenhagen, R. Bolli, T. Braun, L. J. Field, B. K. Fleischmann, J. Frisen, M. Giacca, J. M. Hare, S. Houser, R. T. Lee, E. Marban, J. F. Martin, J. D. Molkentin, C. E. Murry, P. R. Riley, P. Ruiz-Lozano, H. A. Sadek, M. A. Sussman, J. A. Hill, Cardiomyocyte Regeneration: A Consensus Statement. *Circulation* **136**, 680-686 (2017).

30. R. Gallet, J. Dawkins, J. Valle, E. Simsolo, G. de Couto, R. Middleton, E. Tseliou, D. Luthringer, M. Kreke, R. R. Smith, L. Marban, B. Ghaleh, E. Marban, Exosomes

secreted by cardiosphere-derived cells reduce scarring, attenuate adverse remodelling, and improve function in acute and chronic porcine myocardial infarction. *Eur Heart J* **38**, 201-211 (2017).

31. S. C. Saunderson, A. C. Dunn, P. R. Crocker, A. D. McLellan, CD169 mediates the capture of exosomes in spleen and lymph node. *Blood* **123**, 208-216 (2014).

32. L. Barile, V. Lionetti, E. Cervio, M. Matteucci, M. Gherghiceanu, L. M. Popescu, T. Torre, F. Siclari, T. Moccetti, G. Vassalli, Extracellular vesicles from human cardiac progenitor cells inhibit cardiomyocyte apoptosis and improve cardiac function after myocardial infarction. *Cardiovasc Res* **103**, 530-541 (2014).

33. E. Tseliou, J. Fouad, H. Reich, L. Slipczuk, G. de Couto, M. Aminzadeh, R. Middleton, J. Valle, L. Weixin, E. Marban, Fibroblasts Rendered Antifibrotic, Antiapoptotic, and Angiogenic by Priming With Cardiosphere-Derived Extracellular Membrane Vesicles. *J Am Coll Cardiol* **66**, 599-611 (2015).

34. H. Park, X. Huang, C. Lu, M. S. Cairo, X. Zhou, MicroRNA-146a and microRNA-146b regulate human dendritic cell apoptosis and cytokine production by targeting TRAF6 and IRAK1 proteins. *J Biol Chem* **290**, 2831-2841 (2015).

35. Y. Zhang, X. H. Feng, R. Derynck, Smad3 and Smad4 cooperate with c-Jun/c-Fos to mediate TGF-beta-induced transcription. *Nature* **394**, 909-913 (1998).

36. L. Song, M. Su, S. Wang, Y. Zou, X. Wang, Y. Wang, H. Cui, P. Zhao, R. Hui, J. Wang, MiR-451 is decreased in hypertrophic cardiomyopathy and regulates autophagy by targeting TSC1. *J Cell Mol Med* **18**, 2266-2274 (2014).

37. Y. Kuwabara, T. Horie, O. Baba, S. Watanabe, M. Nishiga, S. Usami, M. Izuhara, T. Nakao, T. Nishino, K. Otsu, T. Kita, T. Kimura, K. Ono, MicroRNA-451 exacerbates lipotoxicity in cardiac myocytes and high-fat diet-induced cardiac hypertrophy in mice through suppression of the LKB1/AMPK pathway. *Circ Res* **116**, 279-288 (2015).

38. P. Saha, S. Sharma, L. Korutla, S. R. Datla, F. Shoja-Taheri, R. Mishra, G. E. Bigham, M. Sarkar, D. Morales, G. Bittle, M. Gunasekaran, C. Ambastha, M. Y. Arfat, D. Li, A. Habertheuer, R. Hu, M. O. Platt, P. Yang, M. E. Davis, P. Vallabhajosyula, S. Kaushal, Circulating exosomes derived from transplanted progenitor cells aid the functional recovery of ischemic myocardium. *Sci Transl Med* **11**, (2019).

39. U. Agarwal, A. George, S. Bhutani, S. Ghosh-Choudhary, J. T. Maxwell, M. E. Brown, Y. Mehta, M. O. Platt, Y. Liang, S. Sahoo, M. E. Davis, Experimental, Systems, and Computational Approaches to Understanding the MicroRNA-Mediated Reparative Potential of Cardiac Progenitor Cell-Derived Exosomes From Pediatric Patients. *Circ Res* **120**, 701-712 (2017).

40. X. Jiang, J. Sucharov, B. L. Stauffer, S. D. Miyamoto, C. C. Sucharov, Exosomes from pediatric dilated cardiomyopathy patients modulate a pathological response in cardiomyocytes. *Am J Physiol Heart Circ Physiol* **312**, H818-H826 (2017).

41. W. Y. Shi, M. Moreno-Betancur, A. W. Nugent, M. Cheung, S. Colan, C. Turner, G. F. Sholler, T. Robertson, R. Justo, A. Bullock, I. King, A. M. Davis, P. E. F. Daubeney, R. G. Weintraub, S. National Australian Childhood Cardiomyopathy, Long-Term Outcomes of Childhood Left Ventricular Noncompaction Cardiomyopathy. *Circulation* **138**, 367-376 (2018).

42. J. I. van Waning, K. Caliskan, M. Michels, A. F. L. Schinkel, A. Hirsch, M. Dalinghaus, Y. M. Hoedemaekers, M. W. Wessels, I. J. AS, R. M. W. Hofstra, M. A. van Slegtenhorst, D. Majoor-Krakauer, Cardiac Phenotypes, Genetics, and Risks in Familial Noncompaction Cardiomyopathy. *J Am Coll Cardiol* **73**, 1601-1611 (2019).

43. J. A. Alvarez, E. J. Orav, J. D. Wilkinson, L. E. Fleming, D. J. Lee, L. A. Sleeper, P. G. Rusconi, S. D. Colan, D. T. Hsu, C. E. Canter, S. A. Webber, G. F. Cox, J. L. Jefferies, J. A. Towbin, S. E. Lipshultz, I. Pediatric Cardiomyopathy Registry, Competing risks for death and cardiac transplantation in children with dilated cardiomyopathy: results from the pediatric cardiomyopathy registry. *Circulation* **124**, 814-823 (2011).

44. K. M. Molina, P. Shrader, S. D. Colan, S. Mital, R. Margossian, L. A. Sleeper, G. Shirali, P. Barker, C. E. Canter, K. Altmann, E. Radojewski, E. S. Tierney, J. Rychik, L. Y. Tani, I. Pediatric Heart Network, Predictors of disease progression in pediatric dilated cardiomyopathy. *Circ Heart Fail* **6**, 1214-1222 (2013).

45. V. O. Puntmann, G. Carr-White, A. Jabbour, C. Y. Yu, R. Gebker, S. Kelle, R. Hinojar, A. Doltra, N. Varma, N. Child, T. Rogers, G. Suna, E. Arroyo Ucar, B. Goodman, S. Khan, D. Dabir, E. Herrmann, A. M. Zeiher, E. Nagel, T. M. C. M. R. O. S. International, T1-Mapping and Outcome in Nonischemic Cardiomyopathy: All-Cause Mortality and Heart Failure. *JACC Cardiovasc Imaging* **9**, 40-50 (2016).

46. F. aus dem Siepen, S. J. Buss, D. Messroghli, F. Andre, D. Lossnitzer, S. Seitz, M. Keller, P. A. Schnabel, E. Giannitsis, G. Korosoglou, H. A. Katus, H. Steen, T1 mapping in dilated cardiomyopathy with cardiac magnetic resonance: quantification of

diffuse myocardial fibrosis and comparison with endomyocardial biopsy. *Eur Heart J Cardiovasc Imaging* **16**, 210-216 (2015).

47. J. A. B. Araujo-Filho, A. N. Assuncao, Jr., M. D. Tavares de Melo, L. Biere, C. R. Lima, R. N. Dantas, Jr., C. H. Nomura, V. M. C. Salemi, M. Jerosch-Herold, J. R. Parga, Myocardial T1 mapping and extracellular volume quantification in patients with left ventricular non-compaction cardiomyopathy. *Eur Heart J Cardiovasc Imaging* **19**, 888-895 (2018).

48. G. Suzuki, R. F. Young, M. M. Leiker, T. Suzuki, Heart-Derived Stem Cells in Miniature Swine with Coronary Microembolization: Novel Ischemic Cardiomyopathy Model to Assess the Efficacy of Cell-Based Therapy. *Stem Cells Int* **2016**, 6940195 (2016).

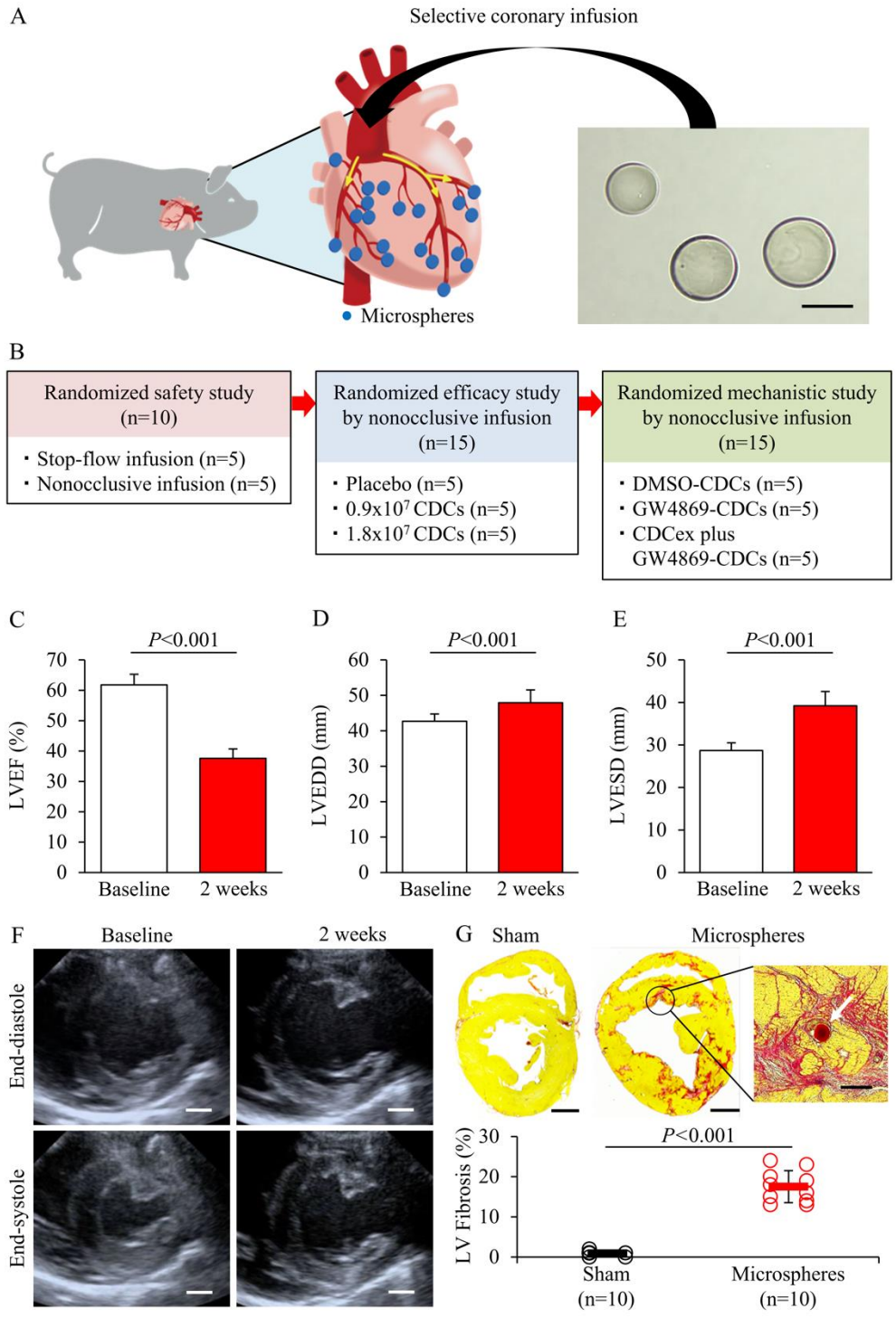

Fig. 1. Generation of a swine model of DCM for randomized preclinical studies.

(A) Schematic and representative brightfield microscopic images of microspheres used for selective coronary injection to achieve global cardiac dysfunction by microembolization. **(B)** Preclinical study design to explore the procedural safety and therapeutic efficacy of intracoronary cardiosphere-derived cell (CDC) infusion in a swine model of DCM. Severely depressed global function **(C)** and dilated ventricular volumes **(D** and **E)** were noted 2 weeks after coronary microembolization (n=40). EDD, end-diastolic dimension. ESD, end-systolic dimension. **(F)** Representative images of echocardiograms during microembolization. **(G)** Picrosirius red staining and quantification of diffuse myocardial fibrosis in swine model of DCM. White arrow in inset shows a microsphere embolized in a capillary vessel. Scale bar, 200 μm in **(A)**; 10 mm in **(F)** and **(G)**; and 300 μm in inset. Data were analyzed using paired *t*-test or Student's *t*-test.

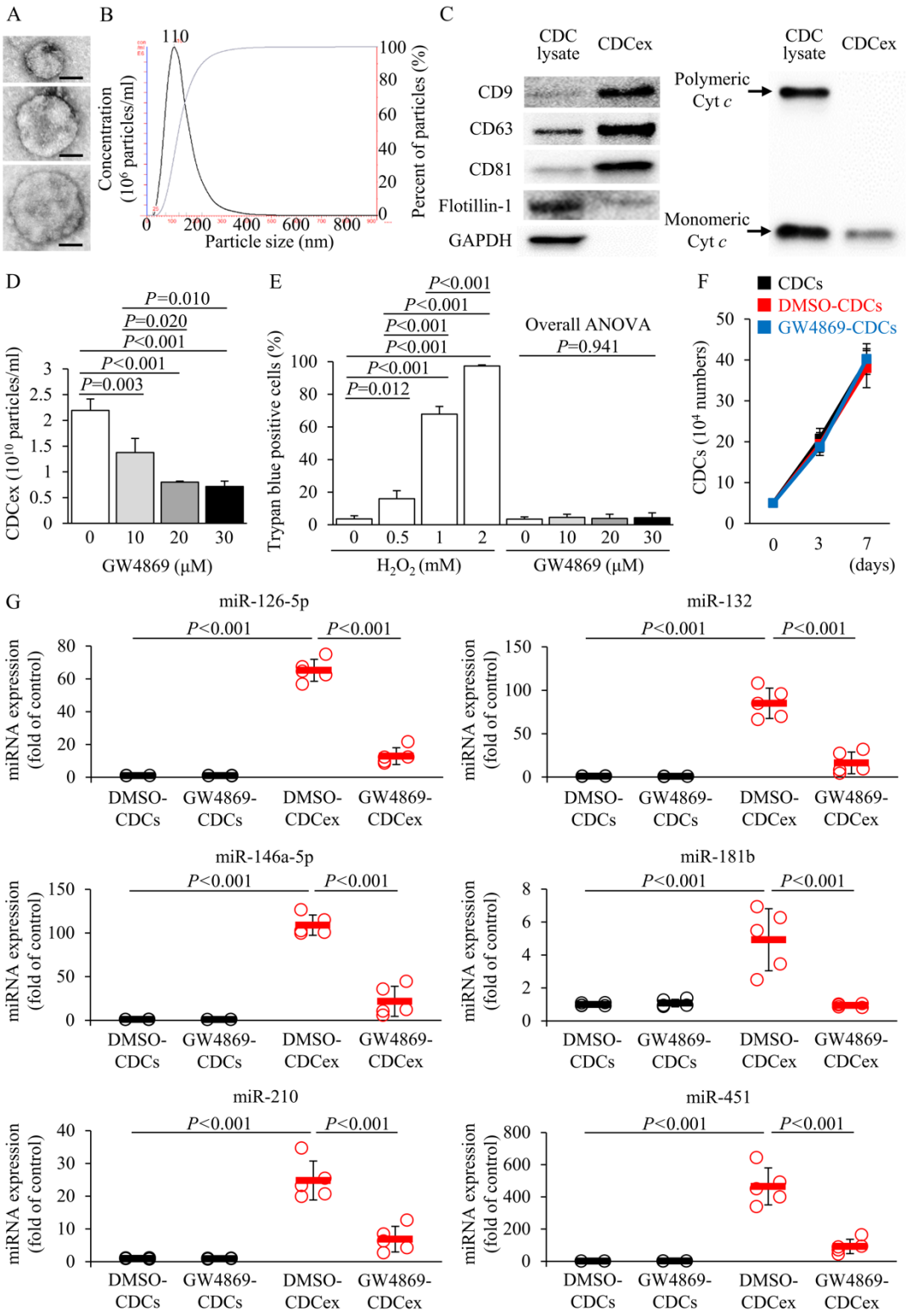

Fig. 2. Exosome isolation and characterization.

(A) Exosomes isolated from porcine CDCs were visualized using an electron microscope. Three different exosomes are shown. Scale bar, 50 nm. **(B)** Size distribution and particle number were assessed by nanoparticle tracking analysis. **(C)** CDCex were verified by immunoblotting of CD9, CD63, CD81, Flotillin-1, and cytochrome *c* (Cyt *c*) and compared with CDC lysate (n≥3). Dose-dependent effects of pre-incubation with GW4869 for 12 hours on **(D)** exosome release in CDCs (n=3), **(E)** CDC viability (n=3), and **(F)** cell growth kinetics in 20 μM GW4869 treatment up to 7 days in culture (n=6). CDCs treated with hydrogen peroxide for 4 hours was used as a positive control. (**G**) CDCs were treated with either DMSO or 20 μM GW4869 for 12 hours and the relative expressions of miRNAs in CDCs and CDCex compared with that of DMSO-treated CDCs were analyzed by real-time RT-PCR (n=5). *Let-7a* was used as an internal control. DMSO, dimethyl sulfoxide. Statistical significance was determined using one-way analysis of variance followed by Tukey post hoc multiple corrections test.

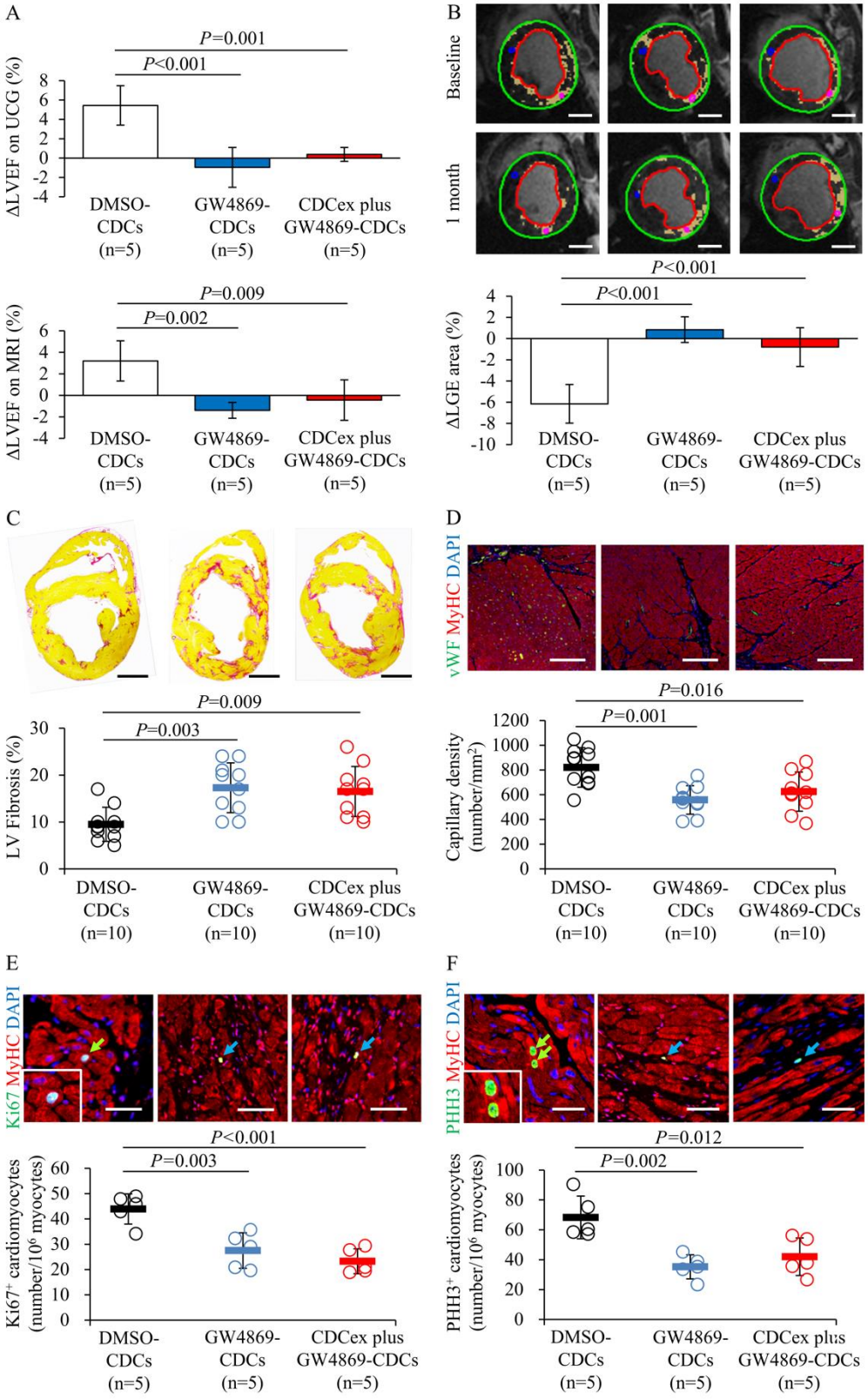

Fig. 3. CDC exosome-mediated cardiac repair in a swine DCM model.

Two weeks after microembolization, DCM pigs were randomly allocated to be treated with 0.9×10^7 CDCs pre-incubated with either DMSO or GW4869 with or without co-injection of CDCex isolated from $0.9x10^7$ CDCs. (**A**) Cardiac function was analyzed 1 month after treatment using ultrasound echocardiogram (UCG, top) and cMRI (bottom). Absolute changes in LVEF from baseline to 1 month of follow-up are shown. Myocardial fibrosis was analyzed using LGE **(B)** and Picrosirius red staining **(C)**. Capillary density and cardiomyocyte proliferation were monitored using von Willebrand factor (vWF, **D**), Ki67 **(E)**, and phospho-histone H3 (PHH3, **F**) immunofluorescence in hearts after intracoronary injection of 0.9×10^7 CDCs pre-incubated with either DMSO or GW4869 (20 μM) with or without co-injection of CDCex isolated from $0.9x10^7$ CDCs. Heart sections were counterstained with myosin heavy chain (MyHC) to visualize cardiomyocytes and DAPI (4′,6-diamidino-2-phenylindole) nuclear marker. Green arrows show Ki67 or PHH3 positive cardiomyocyte. MyHC negative non-cardiomyocytes expressing either Ki67 or PHH3 were shown by blue arrows. Scale bar, 10 mm in **(B)** and **(C)**; 50 μm in **(D)**; and 200 μm in **(E** and **F)**. Statistical analysis was performed by using one-way analysis of variance followed by Tukey post hoc multiple corrections test.

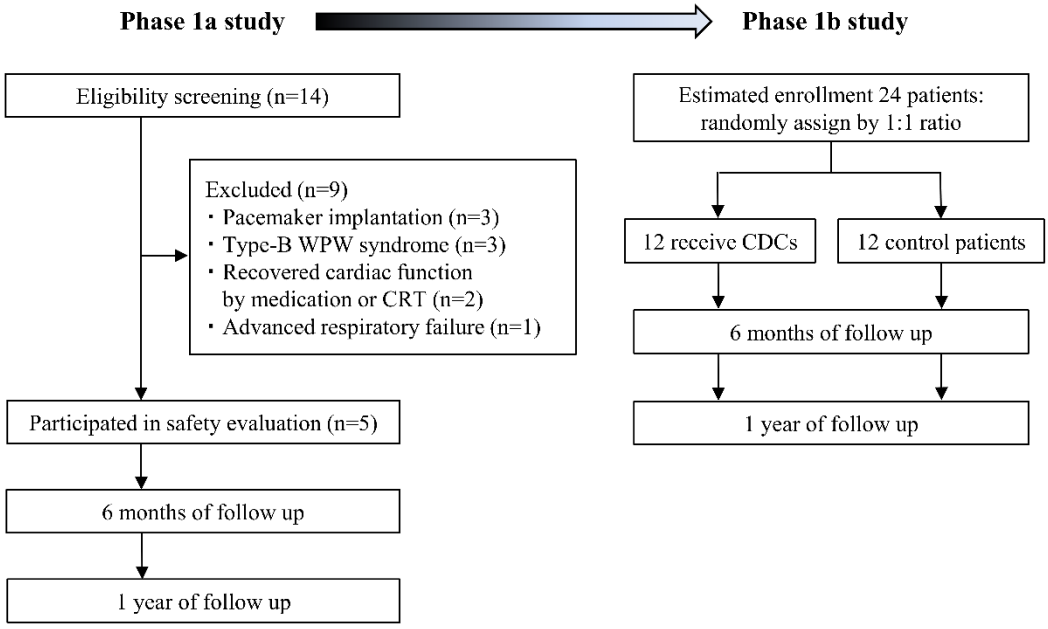

Fig. 4. Study flow chart of TICAP-DCM phase 1 trial.

The TICAP-DCM trial was composed of two stages. The primary objective was to investigate the procedural safety of intracoronary infusion of CDCs (3.0×10^5/kg) by non-stop-flow delivery approach in 5 patients with DCM and reduced ejection fraction as an open-label, lead-in phase 1a study. The second stage was an open-label, randomized-controlled (1:1 ratio) study to evaluate the therapeutic efficacy of CDC infusion in 24 patients with similar eligible criteria (Phase 1b study). The secondary endpoint analysis was to assess the absolute changes in cardiac function and myocardial fibrosis in patients 6 months after CDC treatment compared with control participants treated by standard medication alone. WPW, Wolff–Parkinson–White. CRT, cardiac resynchronization therapy. Recovered cardiac function is determined by LVEF ≥40% during screening.

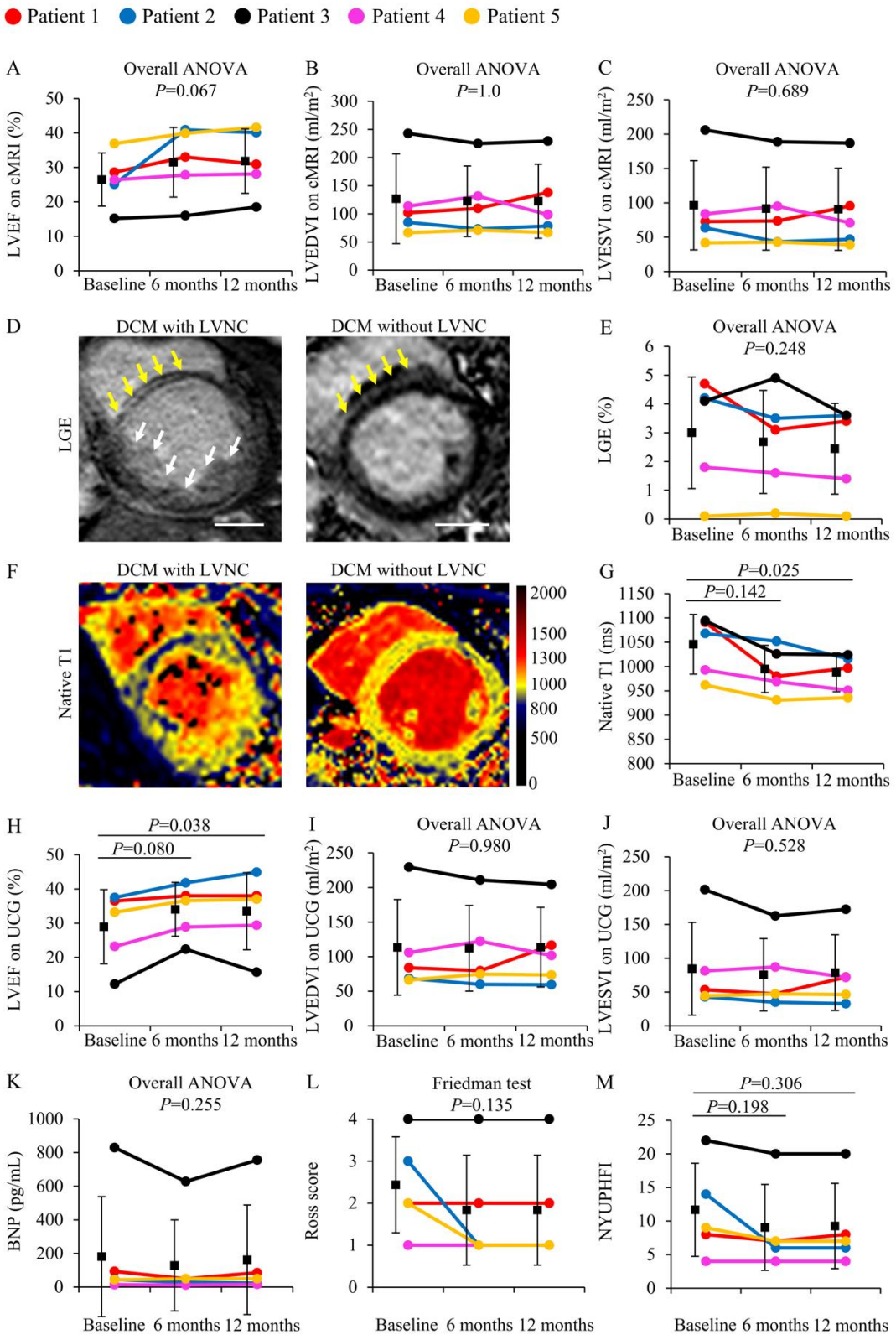

Fig. 5. Cardiac function analysis and heart failure status in the TICAP-DCM phase 1a trial (secondary efficacy outcomes).

(A to **C)** Ventricular function and end-diastolic and end-systolic volumes were assessed using cMRI from baseline over 12 months. EDVI, end-diastolic volume index. ESVI, end-systolic volume index. Individual participant data are shown. Myocardial fibrosis was analyzed using LGE **(D)** and native T1 mapping **(F)** in DCM patients with or without LVNC. **(D)** Mid-wall fibrosis was detected using LGEs with mid-myocardial distribution in the interventricular septum and highlighted with yellow arrows. The deep intertrabecular recesses in a DCM patient with LVNC are shown (white arrows). Scale bar, 20 mm. **(E)** Regional myocardial fibrosis was analyzed using the extent of LGE in 5 patients treated by CDC infusion from baseline to 12 months of follow-up. **(F)** Representative images of native T1 mapping revealed prominent trabeculations and interventricular recesses in a DCM patient with LVNC. **(G)** Diffuse myocardial fibrosis was evaluated using native T1 mapping in 5 study participants from baseline to 12 months after CDC treatment. **(H** to **J)** Left ventricular function and volumes were assessed using an echocardiogram from baseline over 12 months after protocol treatment. Heart failure status was monitored by plasma BNP concentrations **(K)**, Ross score **(L)**, and NYUPHFI classification **(M)** from baseline to 12 months of follow-up. Data were analyzed by one-way analysis of variance with repeated measures followed by Dunn–Bonferroni post hoc corrections test or Friedman test followed by Wilcoxon signed-rank test with Dunn–Bonferroni post hoc corrections.

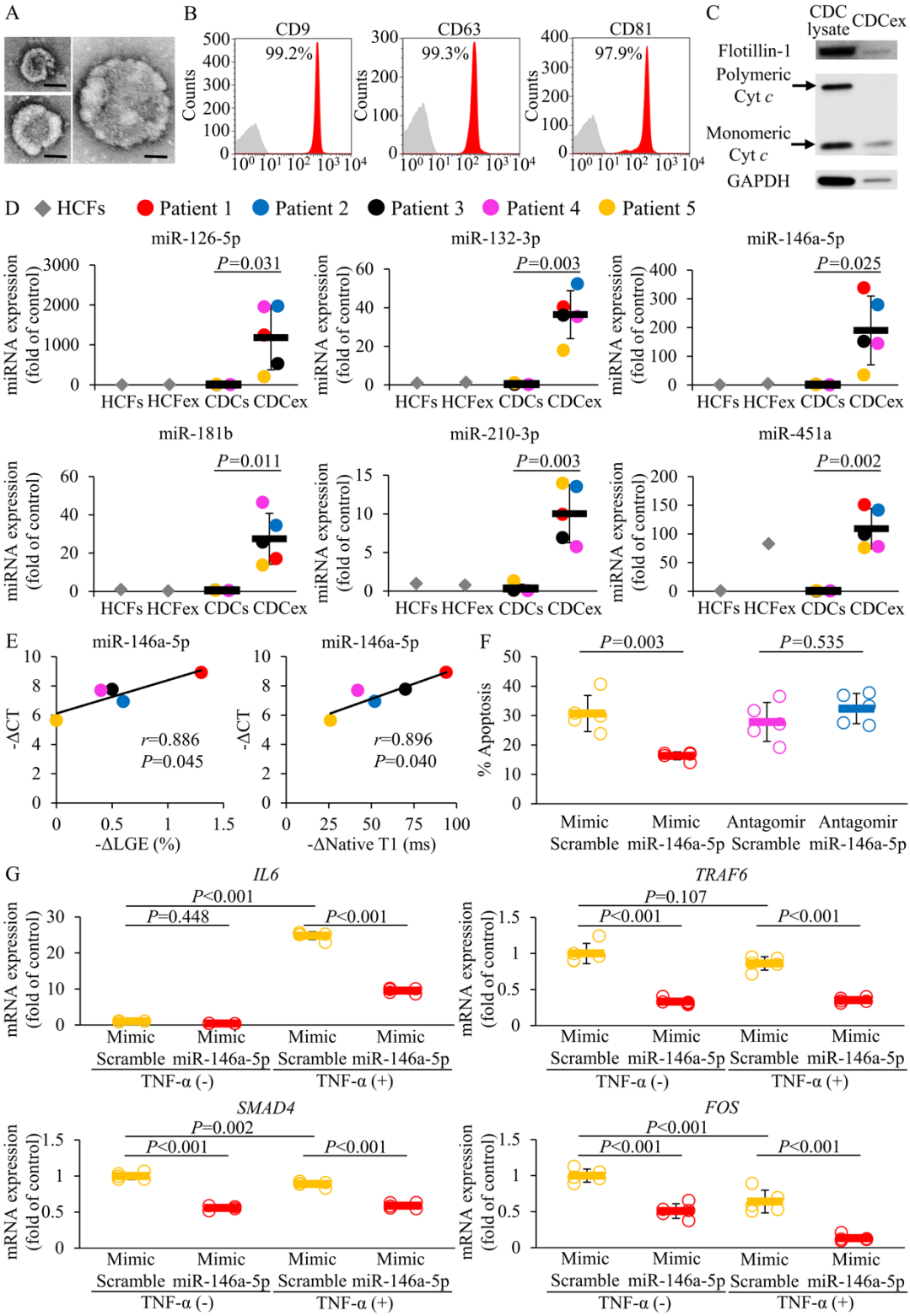

Fig. 6. miR-146a-5p reduced myocardial inflammation and apoptosis through downregulation of *TRAF6/SMAD4/FOS* post-transcripts in human cardiomyocytes.

Exosomes were isolated from study participant-derived CDCs and characterized by transmission electron microscopy **(A)**, flow cytometry **(B)** and immunoblotting **(C)**. Representative images are shown. Scale bar, 50 nm in **(A)**. **(D)** Relative miRNA expression in human CDCs and CDCex from individual patient compared to that of human cardiac fibroblasts (HCFs) are shown (n=5). *U6* was used as an internal reference for normalization. **(E)** Correlations between the changes in myocardial fibrosis (-ΔLGE) or extracellular volume fraction (-ΔNative T1) in individual participants at 12 months compared with baseline and CDCex-derived miR-146a-5p expression relative to *U6* (-ΔCT) are shown. **(F)** Human cardiomyocyte apoptosis was assessed by FACS in AC16 cells treated with TNF-α (200 ng/mL) for 48 hours after transduction of either mimic miR-146a-5p, antagomir to miR-146a-5p, or scramble as corresponding transfection controls (n=5). **(G)** Post-transcriptional regulation of miR-146a-5p targeting downstream effectors were analyzed by real-time RT-PCR in human AC16 cardiac cells treated with or without TNF-α (100 ng/mL) for 24 hours (n=5). Human *β2-microgloblin* was used as an internal control. Statistical significance was determined using paired *t*-test or one-way analysis of variance followed by Tukey multiple comparisons. The linear trend was analyzed by linear regression analysis using Pearson's correlation coefficient.

Table 1. Characteristics of study participants in TICAP-DCM phase 1a trial.

Patient number	Age	Diagnosis	Age at Diagnosis	Ross Classification	Baseline LVEF	BNP (pg/ml)	Medications
1	7 years, 10 months	DCM with LVNC	2 months	II	36.5	93.4	Carvedilol; enalapril; aspirin; torsemide
2	15 years, 5 months	DCM without LVNC	14 years, 9 months	III	37.5	45.2	Carvedilol; enalapril; heparin; furosemide; spironolactone; dobutamine; olprinone
3	14 years, 7 months	DCM without LVNC	12 years, 4 months	IV	12.2	829.7	Carvedilol; enalapril; heparin; furosemide; eplerenone; pimobendan; dobutamine; olprinone
4	17 years, 10 months	DCM without LVNC	6 years, 11 months	I	23.2	14.9	Carvedilol
5	1 years, 5 months	DCM with LVNC	3 months	II	33.2	42.8	Carvedilol; furosemide; spironolactone

BNP, B-type natriuretic peptide; LVNC, left ventricular noncompaction.

Table 2. Adverse events in the TICAP-DCM phase 1a trial (primary endpoint analysis).

	Patients (n=5)
Periprocedural death	0
Periprocedural ST elevation	1
Periprocedural BP↓ (>20 mmHg)	0
Periprocedural ventricular arrhythmia	0
Overall deaths	0
Heart failure	1
Myocardial infarction	0
Ventricular tachycardia >30 seconds	0
Transient ECMO support	1
Infection	1
Incident malignancy	0

BP, blood pressure; ECMO, extracorporeal membrane oxygenation.

Supplementary Materials for

Cardiosphere-derived exosomal microRNAs in pediatric dilated cardiomyopathy

Kenta Hirai[1], Daiki Ousaka[2], Yosuke Fukushima[1], Maiko Kondo[1], Takahiro Eitoku[1], Yusuke Shigemitsu[1], Mayuko Hara[1], Kenji Baba[1], Tatsuo Iwasaki[3], Shingo Kasahara[2], Shinichi Ohtsuki[1], and Hidemasa Oh[4]*

*Corresponding author Email: hidemasa@okayama-u.ac.jp

The PDF file includes:

Materials and Methods

Fig. S1. Isolation, expansion, and characterization of swine CDCs.

Fig. S2. Cardiac enzyme measurements during occlusive or nonocclusive delivery of CDCs in pigs.

Fig. S3. Dose-escalation study to assess CDC-mediated myocardial repair.

Fig. S4. Effects of GW4869 and HIF-1 inhibitor on exosome release and growth factors secretion to modulate adaptive responses to hypoxia.

Fig. S5. Hypoxic CDCs enhanced secretory miRNAs expressions those were repressed by GW4869 and ACF treatment.

Fig. S6. Isolation, expansion, and validation of human CDCs from endomyocardial biopsy specimens.

Fig. S7. Cardiac enzymes and tumor markers measurements for safety profile analysis (primary endpoint measures).

Fig. S8. The impact of miR-146a-5p on TNF-α-mediated autocrine and paracrine signaling against apoptosis in human cardiomyocytes.

Table S1. Adverse events during CDC delivery in swine model of DCM.

Table S2. Inclusion and exclusion criteria of the TICAP-DCM trial.

Table S3. Characteristics of study participants in the TICAP-DCM phase 1a trial.

Table S4. Taqman primers used for CDC and CDCex validation and function.

References (*49*)

Other Supplementary Materials for this manuscript includes the following:

Data file S1 (Microsoft Excel format). Individual subject-level data (separate file).

Materials and Methods

Cardiac function analysis

Echocardiography was performed to assess LV function in pigs using an Aplio300 (Toshiba Medical Systems) with a 5 MHz sector transducer. Cardiac magnetic resonance imaging (cMRI) was performed using a 1.5-Tesla scanner with 8-channel cardiac array coil (GE Healthcare). Contiguous short-axis cine images from the cardiac base to apex were acquired to quantify LV volume and function using a steady-state-free precession sequence (parameters: TR 3.6 msec; TE 1.6 msec; field of view 30×30 cm; slice thickness 8 mm; gap 0 mm; data matrix 224×224; and flip angle 45°) and then analyzed on a commercially available workstation cvi42 (Circle Cardiovascular Imaging Inc).

LGE images were acquired 10 minutes after intravenous injection of gadoteridol (0.2 mM/kg body weight; ProHance: Eisai) using an electrocardiogram-gated inversion recovery T1 turbo field echo sequence (parameters: TR 6.6 msec; TE 3.2 msec; field of view 30×22.5 cm; slice thickness 8 mm; gap 0 mm; data matrix 256×192; and flip angle 20°). The extent of enhanced myocardium was assessed on a 17-segment cardiac model using short axis slices and defined by a semi-automatic thresholding method as myocardium with a signal intensity cut-off value of 5 or more standard deviations (SDs) above the mean of remote myocardium (*7*). All images underwent blinded evaluation by two experienced operators.

Cell culture

Human CDCs were generated from right ventricular endomyocardial biopsy specimens, expanded in Dulbecco's modified Eagle medium (DMEM)/F12 medium containing 10% fetal bovine serum (FBS; Sigma-Aldrich), 20 ng/mL epidermal growth factor (Wako Co. Ltd.), and

40 ng/mL basic fibroblast growth factor (Wako Co. Ltd.) at a Good Manufacturing Practice facility in Okayama University Hospital, and characterized as described previously (*5, 12*). In animal experiments, allogeneic CDCs were isolated and manufactured from 5 independent male porcine donors at an age of 8-week-old. The right atrial tissue was surgically collected from Yorkshire pigs, cut into small pieces, and grown as explant cultures on dishes (Falcon, 353004) in Iscove's modified Dulbecco's medium (IMDM; Thermo Fisher Scientific) containing 20% FBS, 2 mM L-glutamine (Thermo Fisher Scientific), 0.1 mM 2-mercaptoethanol (Wako Co. Ltd.), and 1% penicillin and streptomycin (Thermo Fisher Scientific). The cells surrounding the adherent explants were then harvested and reseeded at 5×10^4 cells/mL onto poly-D-lysine-coated dishes. After several days, detached cardiospheres were collected and expanded in 20% FBS containing IMDM on culture dishes (Falcon, 353003). Human cardiac fibroblasts (HCFs; PromoCell) were purchased and cultured on dishes (Falcon, 353003) with fibroblast growth medium 3 (PromoCell).

Transfection and hypoxia

Undifferentiated human AC16 cells (Millipore) were maintained in DMEM/F12 supplemented with 12.5% FBS and were transfected with mimic miR-146a-5p (MC10722), antagomir to miR-146a-5p (MH10722), or corresponding negative controls (mirVana miRNA mimic negative control and mirVana miRNA inhibitor negative control; all purchased from Invitrogen) using lipofectamine RNAiMAX in serum-free Opti-MEM medium (Thermo Fisher Scientific). Transfection efficiency was determined 24 hours after transfection by real-time RT-PCR. Hypoxic condition was conducted at 37^0C in a hypoxic workstation (BIONIX-3 hypoxic culture kit; Sugiyamagen) in an atmosphere containing 5% CO_2 balanced with nitrogen to reach oxygen

concentration at 1% for 12 hours. Normoxic cell culture was performed in a standard incubator containing 5% CO_2 and 20% oxygen.

Isolation of mRNAs and miRNAs

Total RNA was extracted using TRIzol (Thermo Fisher Scientific) and used to synthesize cDNA with a QuantiTect Reverse Transcription Kit (QIAGEN). Small RNA of CDCs and CDCex was isolated using a mirVana PARIS kit (Life Technologies Co.) according to the manufacturer's protocol. Four hundred μl of disruption buffer was added to the cells or exosomes, and lysed with an equal volume of denaturing solution. After an acid phenol chloroform extraction, the sample tube was centrifuged at 20,000 rpm for 10 min at 4°C. The aqueous phase was carefully transferred, mixed with 100% ethanol, and passed two times through a mirVana PARIS filter cartridge. Small RNA was eluted in 100 μl of preheated elution solution.

Real-time RT-PCR

mRNA expression was analyzed by real-time reverse transcription polymerase chain reaction (RT-PCR) with pig / human *β2-microglobulin* (*B2M*) or human-specific *β-actin* (*ACTB*) primers and probes (table S4) using Taqman Universal PCR Master Mix (Applied Biosystems), as described previously (*5*). Taqman MicroRNA assays were performed using a TaqMan MicroRNA RT kit (Thermo Fisher Scientific) with small RNA primers (table S4) according to manufacturer's protocol. *Let-7a* and *U6* were used as invariant controls for pig and human studies, respectively.

Native T1 mapping

Cardiac functions for trial participants were analyzed using Doppler echocardiogram (EPIQ 7G; Philips Healthcare) and cMRI (Siemens 1.5 Tesla MAGNETOM Aera; Siemens AG) with single-breath-hold modified Look-Locker inversion recovery sequence and the dichotomous variables for presence or absence of LGE were determined quantitatively, as described previously (*6, 7*). The native T1 values were determined by manual tracing of the compacted myocardial layers located in the regions with or without prominent trabeculations in every single segment of 3 short-axis imaging planes of mid-ventricle using 16-segmental analysis (*49*).

Growth factor measurement

The concentration of bFGF in conditioned medium was measured by using enzyme linked immunosolvent assay kit (NBP-69961, Novus Biologicals). Concentrations of VEGF and IGF1 in culture medium were determined by commercially available enzyme immunoassay (LSI Medience) and radioimmunoassay (SRL) kits, respectively.

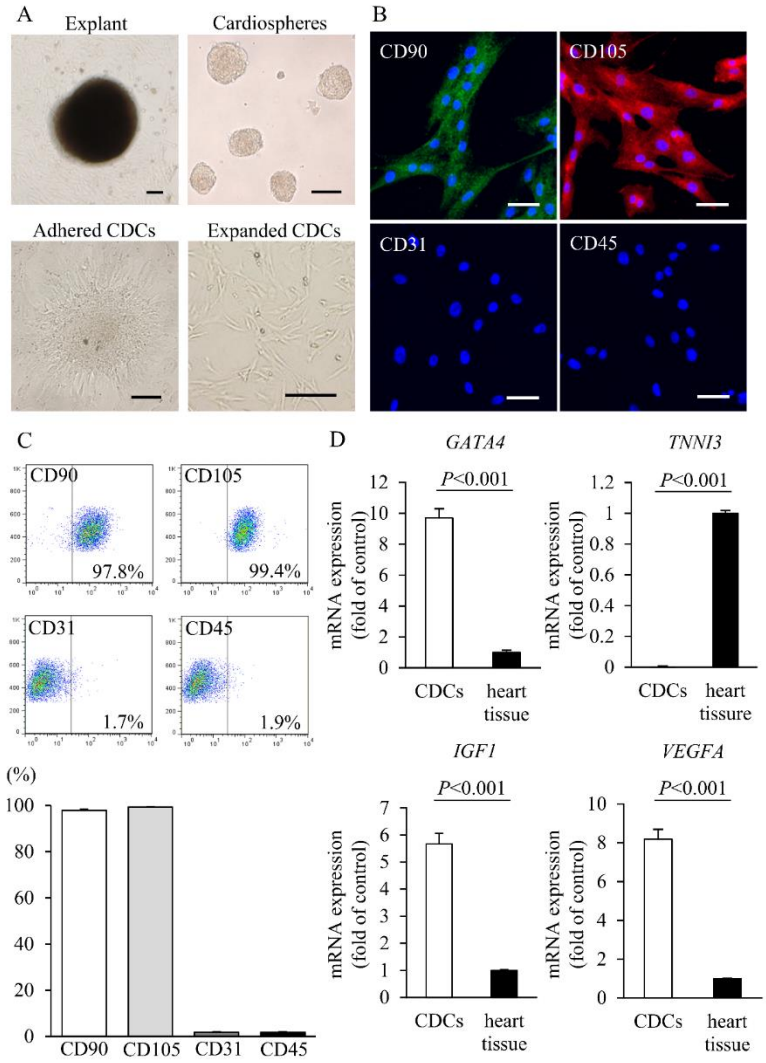

Fig. S1. Isolation, expansion, and characterization of swine CDCs.

(A) Surgically collected right atrial tissues were cut into small pieces and grown as an explant culture. Harvested explants were reseeded onto poly-D-lysine-coated plates to generate self-assembly of cardiospheres. CDCs were obtained by reseeding and expanding the cardiospheres in adherent culture. **(B** and **C)** Immunofluorescence and FACS analysis of swine CDCs for expression of CD90, CD105, CD31, and CD45. **(D)** Cardiac progenitor potential verified by mRNA expression of cardiac transcription factors, myocardial structural genes, and growth factors by real-time RT-PCR. A pig *β2-microgloblin* was used as a housekeeping gene. Swine heart tissue was used as control. All experiments were repeated more than three times with similar results. Scale bar, 100 μm in **(A)**; and 50 μm in **(B)**. Data were analyzed using Student's *t*-test.

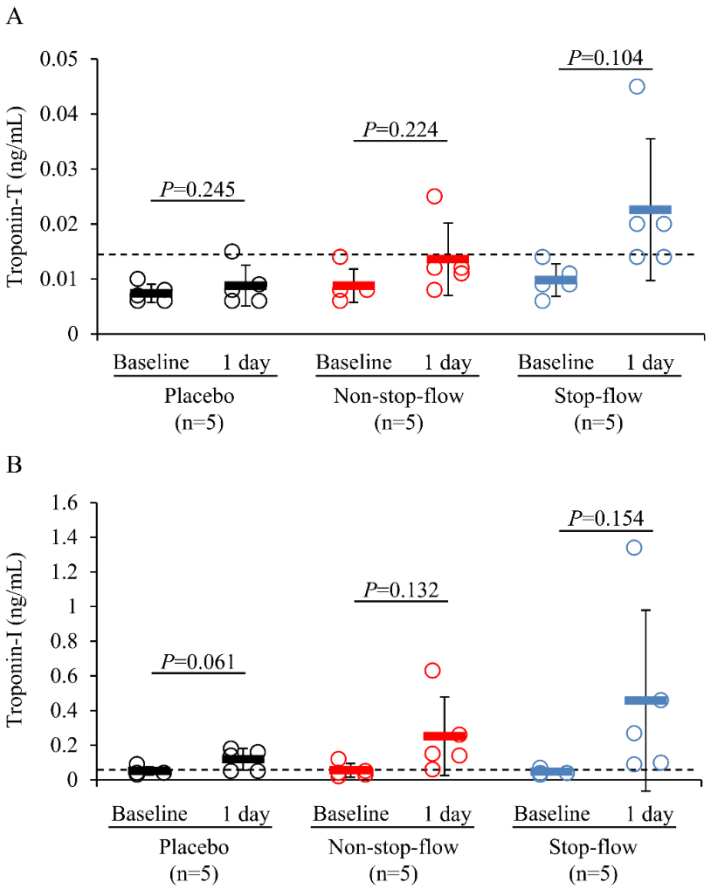

Fig. S2. Cardiac enzyme measurements during occlusive or nonocclusive delivery of CDCs in pigs.

Two weeks after microembolization, a swine model of DCM was randomly subjected to treatment with intracoronary infusion of 0.9×10^7 CDCs suspended in 15 mL with or without a stop-flow procedure. Serum cardiac troponin-T **(A)** and troponin-I **(B)** were measured before and 1 day after delivery. The same amount of intracoronary PBS injection was set as placebo control independent of randomization for reference. Dashed lines represent the upper normal limits. Statistical significance was determined using paired *t*-test.

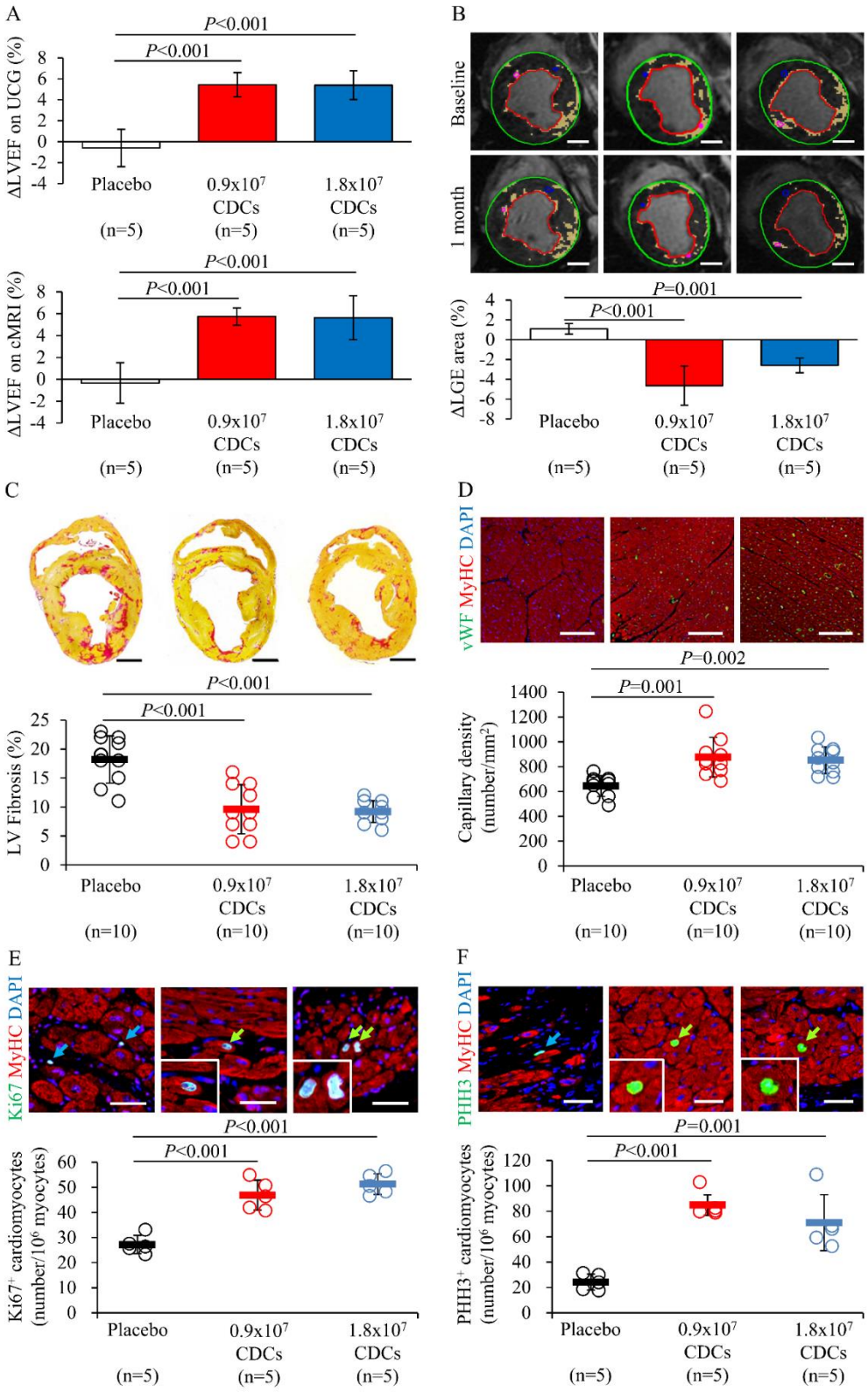

Fig. S3. Dose-escalation study to assess CDC-mediated myocardial repair.

(**A**) Randomized preclinical study in a swine model of DCM. DCM pigs were randomly assigned to receive placebo, 0.9×10^7 CDCs, or 1.8×10^7 CDC infusion. CDCs were delivered into three coronary arteries by nonocclusive infusion, and their therapeutic effects were compared with placebo injection. Cardiac function was assessed by ultrasound echocardiogram (UCG, top) and cMRI (bottom). Absolute changes in LVEF from baseline to 1 month after treatment as indicated are shown. **(B** and **C)** Myocardial fibrosis was analyzed at 1 month post treatment by late gadolinium enhancement (LGE) and Picrosirius red staining. Heart sections were stained with myosin heavy chain (MyHC) and von Willebrand factor (vWF, **D**), Ki67 **(E)**, or phospho-histone-H3 (PHH3, **F**) to evaluate neovascularization and cardiomyocyte proliferation. Green arrows show Ki67 or PHH3 positive cardiomyocyte. MyHC negative non-cardiomyocytes expressing either Ki67 or PHH3 were shown by blue arrows. Scale bar, 10 mm in **(B)** and **(C)**; 50 μm in **(D)**; and 200 μm in **(E** and **F)**. Statistical significance was determined using one-way analysis of variance followed by Tukey multiple corrections test.

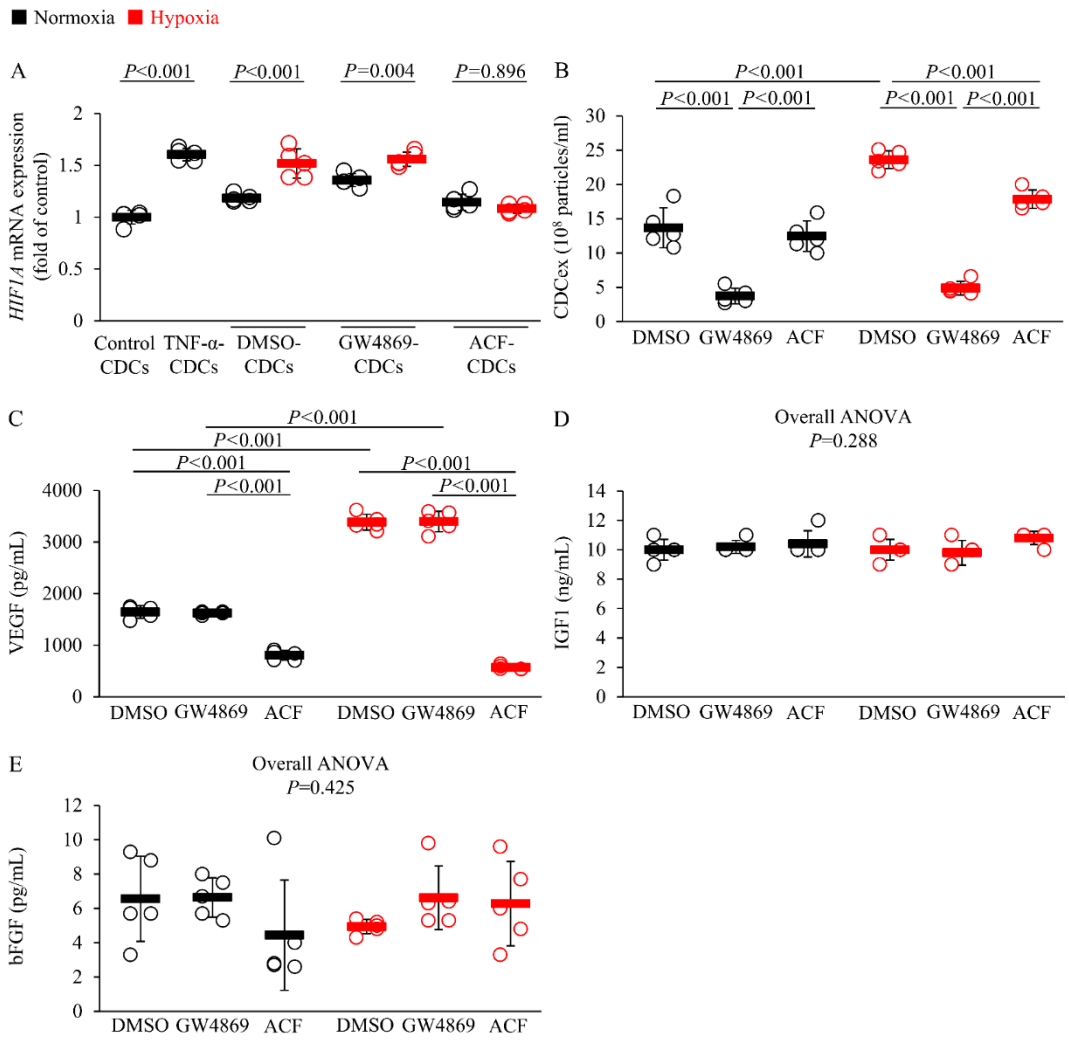

Fig. S4. Effects of GW4869 and HIF-1 inhibitor on exosome release and growth factors secretion to modulate adaptive responses to hypoxia.

(A) Swine CDCs were pretreated with DMSO, GW4869, or acriflavine (ACF, HIF-1 inhibitor) for 12 hours and cultured for additional 1 hour under normoxic or hypoxic conditions; *HIF-1A* transcriptional expression was analyzed. CDCs treated with TNF-α (100 ng/mL) for 1 hour were shown as a positive control. **(B)** CDCex release assessed by nanoparticle tracking analysis in either normoxic or hypoxic conditioning for 12 hours in CDCs pretreated with DMSO, GW4869, or ACF. Proangiogenic growth factor, VEGF **(C)** and IGF1 **(D)** and bFGF **(E)** secretion from CDCs with DMSO, GW4869, or ACF treatment in either oxygen condition for 12 hours. A pig *β2-microgloblin* was used as a housekeeping gene. Statistical significance was determined using one-way analysis of variance followed by Tukey post hoc corrections test.

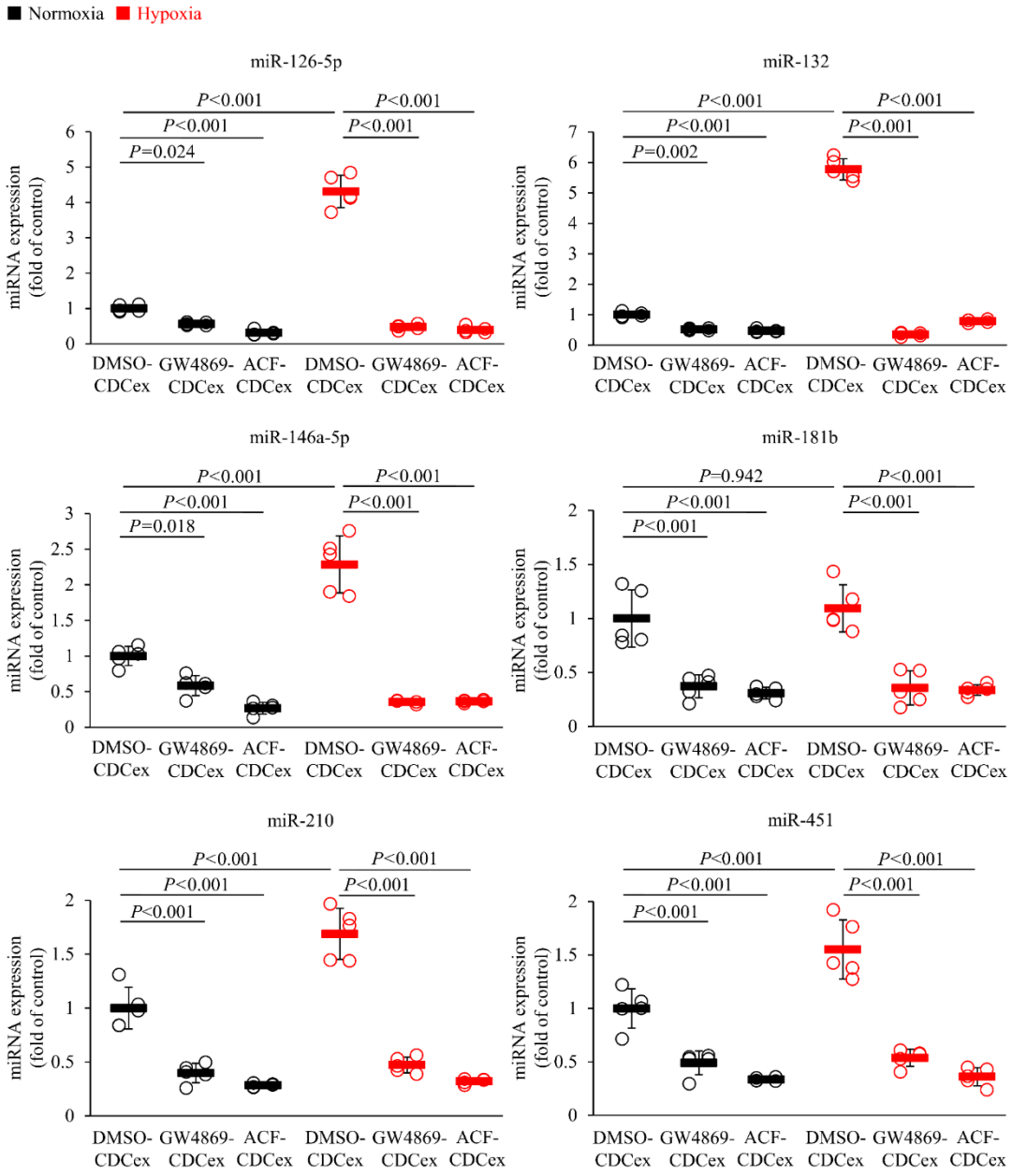

Fig. S5. Hypoxic CDCs enhanced secretory miRNA expression that was repressed by GW4869 and ACF treatment.

Swine CDCs pretreated with DMSO, GW4869, or ACF were cultured for 12 hours as indicated oxygen conditions. The regulatory effects of GW4869 and ACF on CDCex-derived miRNAs were analyzed by real-time RT-PCR (n=5). *Let-7a* was used as an internal control. Statistical significance was determined using one-way analysis of variance followed by Tukey post hoc corrections test.

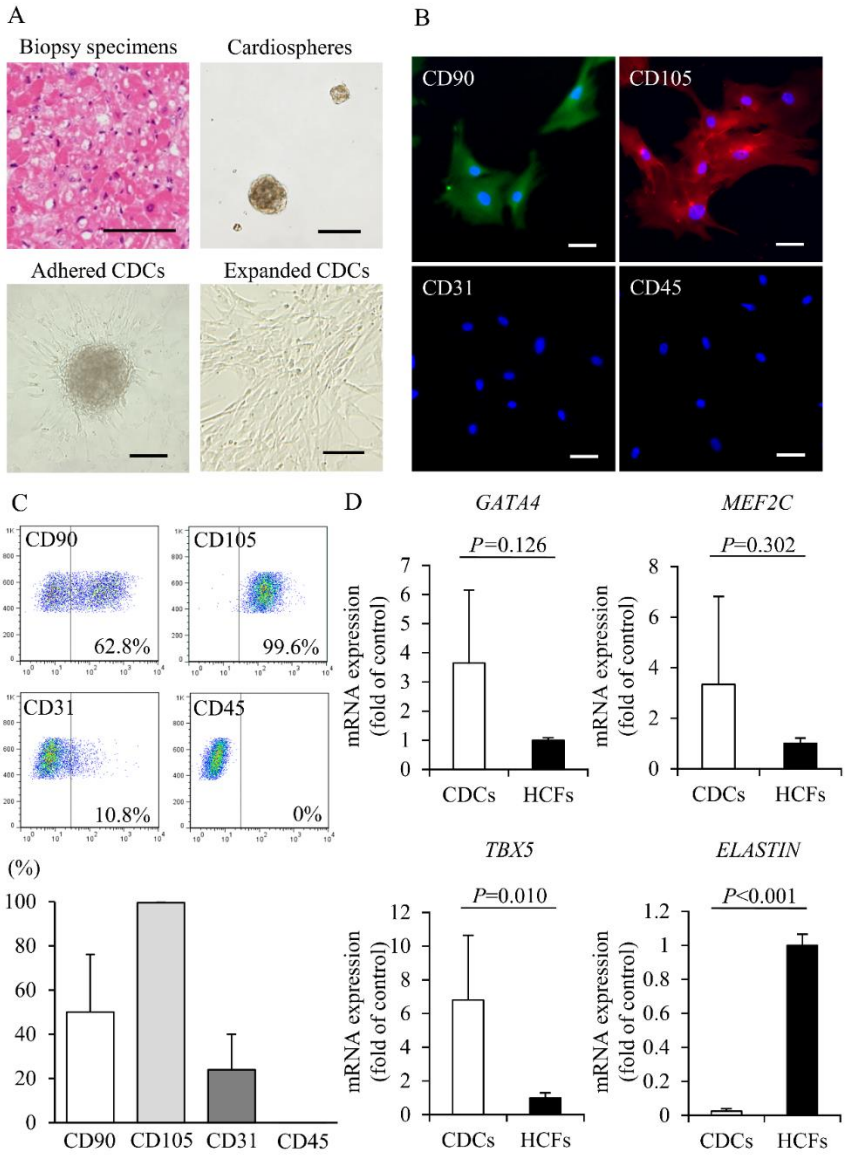

Fig. S6. Isolation, expansion, and validation of human CDCs from endomyocardial biopsy specimens.

(A) Endomyocardial biopsy specimens from right ventricle were stained with H&E staining to establish a diagnosis. Fibrous infiltration and replacement of the myocardium are shown. Human CDCs were isolated from cardiospheres obtained by explant outgrowth and re-plated on adherent conditions for expansion to yield a prespecified dose of CDCs. **(B** and **C)** Quality control validation of CDCs by immunofluorescence and FACS analysis. **(D)** Cardiac transcription factors were examined by real-time RT-PCR. Human cardiac fibroblasts (HCFs) were used for comparison. Human-specific *β-actin* was used as an internal control. Scale bar, 100 μm in **(A)**; and 50 μm in **(B)**. Data were analyzed using Student's *t*-test.

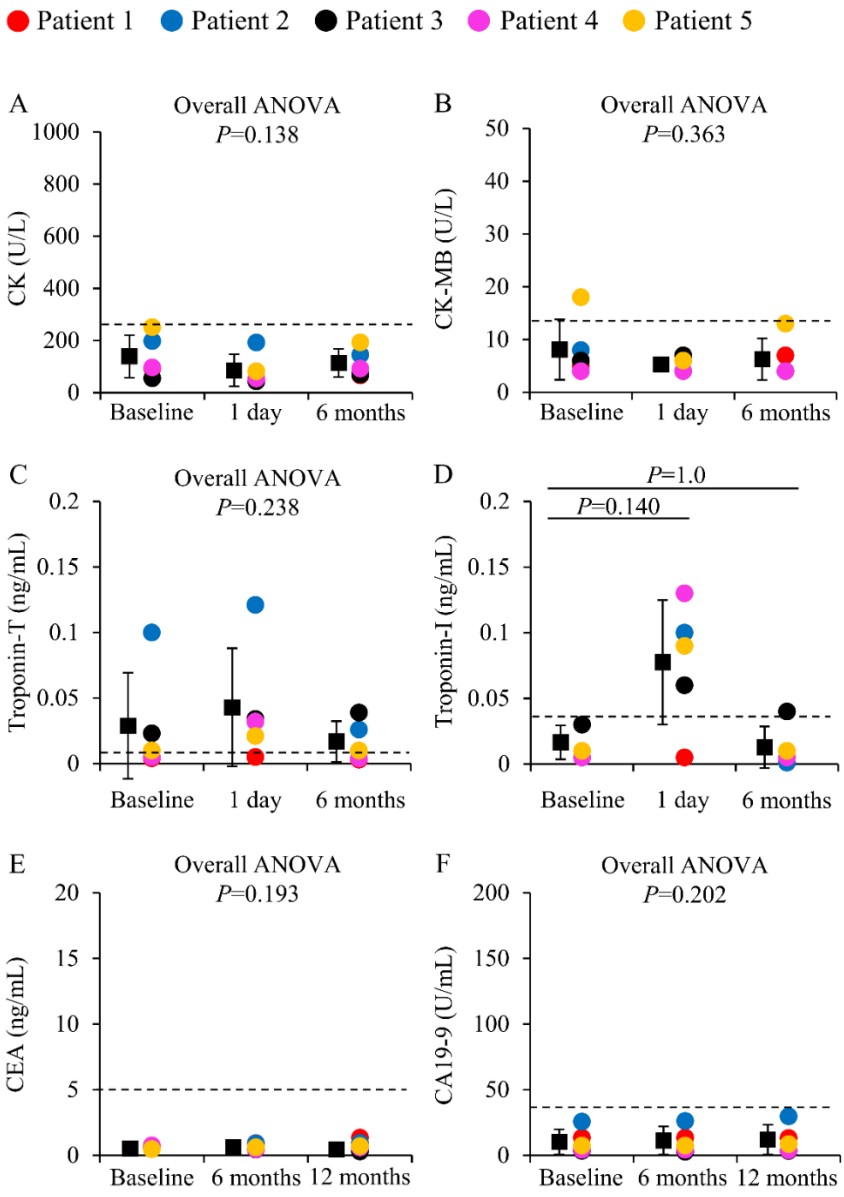

Fig. S7. Cardiac enzymes and tumor markers measurements for safety profile analysis (primary endpoint measures).

Serum creatine kinases **(A** and **B)** and serum cardiac troponin-T and -I **(C** and **D)** were examined at baseline, 1 day, and 6 months after CDC infusion. Individual participant data are shown. **(E** and **F)** Tumor marker measurements during 12 months of follow-up. Dashed lines represent the upper normal limits. Statistical significance was determined using one-way analysis of variance with repeated measures followed by Dunn-Bonferroni post hoc corrections tests.

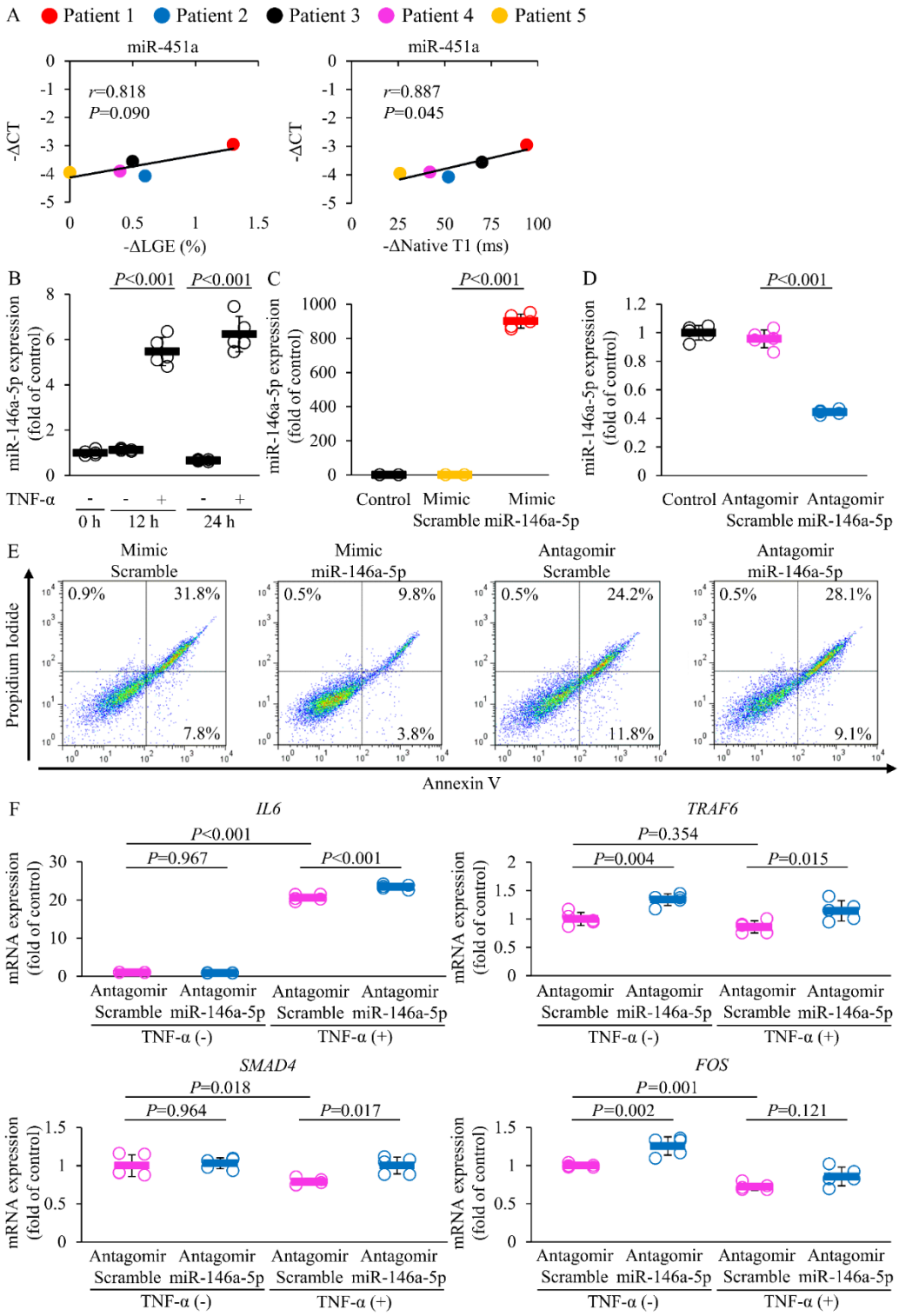

Fig. S8. The impact of miR-146a-5p on TNF-α-mediated autocrine and paracrine signaling against apoptosis in human cardiomyocytes.

(A) Correlations between the CDCex-miR-451a expression relative to *U6* (-ΔCT) and changes in myocardial fibrosis (-ΔLGE) or extracellular volume fraction (-ΔNative T1) in 5 study

participants at 12 months compared with baseline. **(B)** miR-146a-5p expression in human AC16 cardiomyocytes treated with TNF-α (100 ng/mL). **(C** and **D)** Verification of miR-146a-5p overexpression and antagonizing efficiency by transduction of either mimic, antagomir, or respective transfection control against miR-146a-5p in AC16 cardiac cells. Cells without transfection were used as controls. **(E)** TNF-α (200 ng/mL) was administered into AC16 cells for 48 hours to induce myocardial apoptosis. The cardioprotective effect conferred by miR-146a-5p overexpression was shown by FACS. **(F)** *IL6*, *TRAF6*, *SMAD4*, and *FOS* expression in the presence or absence of TNF-α (100 ng/mL) in culture for 24 hours (n=5) with or without antagomir to miR-146a-5p. Human *β2-microgloblin* was used as internal control. Data were analyzed using linear regression analysis using Pearson's correlation coefficient or one-way analysis of variance followed by Tukey post hoc corrections test.

Table S1. Adverse events during CDC delivery in swine model of DCM.

	Placebo (n=5)	Non-stop-flow (n=5)	Stop-flow (n=5)	*P* value
Procedural death	0	0	0 (0%)	
ST-T change	0	0	5 (100%)	0.008
VPC	0	0	4 (80%)	0.048
NSVT	0	0	1 (20%)	1.0
BP ↓ >20 mmHg	0	0	1 (20%)	1.0

VPC, ventricular premature contraction; NSVT, non-sustained ventricular tachycardia; BP, blood pressure. Statistical analysis was performed by Fisher exact test between the groups treated by CDCs with or without stop-flow procedure. Placebo controls without randomization were shown as reference. Data are expressed as n (%).

Table S2. Inclusion and exclusion criteria of the TICAP-DCM trial.

Eligibility criteria
1. Patients diagnosed as dilated cardiomyopathy.
2. Patients aged under 18 years old at the time of enrollment.
3. Left ventricular ejection fraction <40%.
Exclusion criteria
1. Contradiction to cardiac magnetic resonance imaging.
2. Cardiogenic shock.
3. A patient dependent on extracorporeal circulation.
4. A patient with lethal or uncontrollable arrhythmia.
5. A patient with coronary artery disease.
6. A patient with brain dysfunction due to circulatory failure.
7. A patient with malignant neoplasm.
8. A patient with serious neurologic disorder.
9. A patient with advanced respiratory failure or pulmonary hypertension.
10. A patient with advanced renal failure.
11. A patient with multiple organ failure.
12. Active infection.
13. Sepsis.
14. Active hemorrhagic disease (e.g. gastrointestinal bleeding, injury).

Table S3. Characteristics of study participants in the TICAP-DCM phase 1a trial.

	Patients (n=5)
Male sex, n	2 (40%)
Age, y	11.4±6.7
Body weight, kg	35.8±19.2
Heart rate, beats/min	98.0±17.0
Systolic blood pressure, mmHg	100.0±7.3
Diastolic blood pressure, mmHg	53.0±6.9
Ross classification	2.4±1.1
NYUPHFI	11.4±6.9
BNP, pg/ml	205.2±350.2
Family history of DCM	0 (0%)
LBBB	0 (0%)
Medication	
Diuretics (%)	4 (80%)
Beta-blocker (%)	5 (100%)
ACEI or ARB (%)	3 (60%)
PDE3 inhibitor (%)	2 (40%)
Dobutamine (%)	2 (40%)
Aspirin (%)	1 (20%)
Warfarin (%)	0 (0%)
Heparin (%)	2 (40%)

NYUPHFI, New York University pediatric heart failure index; BNP, B-type natriuretic peptide; LBBB, *left bundle branch block;* ACEI, angiotensin converting enzyme inhibitor; ARB, angiotensin II receptor blocker; PDE, phosphodiesterase.

Table S4. Taqman primers used for CDC and CDCex validation and function.

mRNA primers		miRNA primers	
Pig ID		Pig and human ID	
GATA4	Ss03383805_u1	hsa-miR-126*	000451
TNNI3	Ss03385977_u1	hsa-miR-132	000457
IGF1	Ss03394499_m1	hsa-miR-146a	000468
VEGFA	Ss03393991_m1	hsa-miR-210	000512
HIF1A	Ss03390447_m1	hsa-miR-451	001141
B2M	Ss03391156_m1	Pig ID	
Human ID		ssc-*let-7a*	000377
GATA4	Hs00171403_m1	ssc-miR-181b	245498_mat
MEF2C	Hs00231149_m1	Human ID	
TBX5	Hs00361155_m1	*U6* snRNA	001973
ELASTIN	Hs00355783_m1	hsa-miR-181b	001098
ACTB	Hs01060665_g1		
IL6	Hs00174131_m1		
TRAF6	Hs00939742_g1		
SMAD4	Hs00929647_m1		
FOS	Hs04194186_s1		
B2M	Hs00187842_m1		

References

49. S. Nakamori, K. Dohi, M. Ishida, Y. Goto, K. Imanaka-Yoshida, T. Omori, I. Goto, N. Kumagai, N. Fujimoto, Y. Ichikawa, K. Kitagawa, N. Yamada, H. Sakuma, M. Ito, Native T1 Mapping and Extracellular Volume Mapping for the Assessment of Diffuse Myocardial Fibrosis in Dilated Cardiomyopathy. *JACC Cardiovasc Imaging* **11**, 48-59 (2018).